JOURNAL OF GEOPHYSICAL RESEARCH, VOL. 114, C00B06, doi:10.1029/2008JC004993, 2009

Planktonic growth and grazing in the Columbia River plume region: A biophysical model study

N. S. Banas,[1] E. J. Lessard,[2] R. M. Kudela,[3] P. MacCready,[2] T. D. Peterson,[4] B. M. Hickey,[2] and E. Frame[5]

Received 30 June 2008; revised 26 November 2008; accepted 6 April 2009; published 23 June 2009.

[1] A four-box model of planktonic nutrient cycling was coupled to a high-resolution hindcast circulation model of the Oregon-Washington coast to assess the role of the Columbia River plume in shaping regional-scale patterns of phytoplankton biomass and productivity. The ecosystem model tracks nitrogen in four phases: dissolved nutrients, phytoplankton biomass, zooplankton biomass, and detritus. Model parameters were chosen using biological observations and shipboard process studies from two cruises in 2004 and 2005 conducted as part of the River Influences on Shelf Ecosystems program. In particular, community growth and grazing rates from 26 microzooplankton dilution experiments were used, in conjunction with analytical equilibrium solutions to the model equations, to diagnose key model rate parameters. The result is a simple model that reproduces both stocks (of nutrients, phytoplankton, and zooplankton) and rates (of phytoplankton growth and microzooplankton grazing) simultaneously. Transient plume circulation processes are found to modulate the Washington-Oregon upwelling ecosystem in two ways. First, the presence of the plume shifts primary production to deeper water: under weak or variable upwelling winds, 20% less primary production is seen on the inner shelf, and 10–20% more is seen past the 100 m isobath. River effects are smaller when upwelling is strong and sustained. Second, increased retention in the along-coast direction (i.e., episodic interruption of equatorward transport) causes a net shift toward older communities and increased micrograzer impact on both the Oregon and Washington shelves from the midshelf seaward.

Citation: Banas, N. S., E. J. Lessard, R. M. Kudela, P. MacCready, T. D. Peterson, B. M. Hickey, and E. Frame (2009), Planktonic growth and grazing in the Columbia River plume region: A biophysical model study, *J. Geophys. Res.*, *114*, C00B06, doi:10.1029/2008JC004993.

1. Introduction

[2] Along the U.S. Pacific Northwest coast, a highly productive upwelling system interacts with a range of mesoscale features: topographic eddies, canyons, macrotidal estuaries, and multiple strong freshwater inputs [*Hickey*, 1989; *Hickey and Banas*, 2003; *MacFadyen et al.*, 2005; *Hickey et al.*, 2009]. This paper describes a new planktonic ecosystem model for the Washington and northern Oregon coasts (Figure 1) developed to examine the biophysical dynamics of the Columbia River plume in summer.

1.1. Columbia River and Coastal Productivity

[3] This study is part of the River Influences on Shelf Ecosystems (RISE) project, a 5 year, interdisciplinary program of observations and modeling focused on the Columbia River plume region. The large-scale winds in this area are highly variable in all seasons. Summer is dominated by southward, upwelling-favorable winds and winter by northward, downwelling-favorable winds, but strong event-scale (2–10 days) reversals are seen year-round [*Halliwell and Allen*, 1984; *Hickey and Banas*, 2003]. As a result, the Columbia River plume is typically bidirectional in summer [*Hickey et al.*, 2005]. Upwelling winds advect the plume south past Oregon and (through Ekman transport) offshore, but downwelling winds advect the plume northward and onshore along the Washington coast. Remnants of northward plume water can be found on the Washington shelf for many days after each downwelling event, in total more than half of a typical summer [*Hickey et al.*, 2005]. Both upwelling and downwelling plumes have complex effects on coastal productivity. The Columbia outflow is a source of macronutrients and micronutrients (moderate levels of nitrogen, high levels of silica and iron [*Bruland et al.*, 2008]). The rotating near-field plume (the

[1]Applied Physics Laboratory, University of Washington, Seattle, Washington, USA.
[2]School of Oceanography, University of Washington, Seattle, Washington, USA.
[3]Ocean Sciences Department and Institute for Marine Sciences, University of California, Santa Cruz, California, USA.
[4]Science and Technology Center for Coastal Margin Observation and Prediction, Oregon Health and Science University, Beaverton, Oregon, USA.
[5]Northwest Fisheries Science Center, NOAA, Seattle, Washington, USA.

0148-0227/09/2008JC004993$09.00

Figure 1. Map of the Columbia River plume region and model domain. The 100 m, 200 m, and 400 m isobaths are marked.

"bulge region") is a recurrent retention feature [*Horner-Devine*, 2008] and incubator for plankton blooms (T. D. Peterson et al., Influence of a recirculating river plume bulge on biogeochemical processes along the Oregon/Washington shelf, paper presented at the 2008 Ocean Sciences Meeting, American Society of Limnology and Oceanography, Orlando, Florida, 2008). Plume presence increases both turbidity and stratification, and thus may affect the availability of light and oceanic nutrients over a large offshore area (under upwelling conditions) or the Washington inner shelf (under downwelling conditions).

[4] *Banas et al.* [2009] suggested, on the basis of a circulation model developed under RISE [*MacCready et al.*, 2009], that another effect of the plume is to increase the dispersive export of inner shelf water to the outer shelf and beyond. This cross-shelf export, caused by entrainment of inner shelf water into transient topographic and plume-derived eddies, interferes with the advection of upwelled water down the Washington shelf into Oregon, and thus may cause retention of biomass north of the river mouth. This would be a partial explanation of a striking, unexplained large-scale pattern discussed by *Ware and Thomson* [2005] [see also *Hickey and Banas*, 2008; *Hickey et al.*, 2009]: between Washington and Oregon, as along the U.S. West Coast as a whole, phytoplankton biomass and primary production increase to the north while upwelling-favorable wind stress increases to the south. This is contrary to the expectation under a simple theory of coastal upwelling.

[5] But are the plume-related, transient circulation patterns described by *Banas et al.* [2009] biologically

significant? How do the relevant physical timescales compare with key biological timescales, i.e., the phytoplankton community growth rate and zooplankton community grazing rate? Quantitatively, how much does the presence of the Columbia River plume affect summer patterns of biomass and primary production? To answer these questions, we added planktonic nutrient cycling to the *MacCready et al.* [2009] circulation model, with particular attention to phytoplankton and zooplankton community rates. The development and validation of this model is the main subject of this paper. We will conclude with a summary quantification of the effect of the plume on integrated primary production.

1.2. Design of Planktonic Ecosystem Models

[6] This study has a methodological motivation as well. Planktonic nutrient-cycling models (generically, nutrient-phytoplankton-zooplankton, or NPZ, models) have been widespread in oceanography for decades [*Gentleman*, 2002]. These models, built on a stock-flux framework, range from very simple (three compartments: N, P, and Z) to very complex (multiple nutrient currencies, many planktonic functional groups, complex formulations for biological fluxes). However, many recent studies cast doubt on the notion of fixing an unsatisfactory model by adding complexity [*Franks*, 2002; *Arhonditsis and Brett*, 2004; *Flynn*, 2005; *Friedrichs et al.*, 2007]. The meta-analysis of 153 modeling studies by *Arhonditsis and Brett* [2004] found that complex models did not on average fit observations better than simple ones. *Friedrichs et al.* [2007] found that models with multiple zooplankton compartments did not necessarily outperform models with single zooplankton compartments, even when biomass data are assimilated. Finally, even when different models produced similar least squares model-data misfits, they often did so via very different element flow pathways, highlighting the need for more comprehensive data sets that uniquely constrain these pathways.

[7] These are troubling conclusions, particularly the point that when a model contains multiple flow pathways that cannot be distinguished with available observations (e.g., phytoplankton to zooplankton to detritus, versus phytoplankton to detritus), then even a rigorous optimization procedure is "bound to fail" [*Fennel et al.*, 2001]. Ambiguity among flow pathways is equivalent to arbitrariness in a model's biological interpretation.

[8] Our model design method is motivated by these cautionary studies, and leads to an optimistic conclusion: that a very simple NPZ-type model can in fact be made to pass diverse, comprehensive validation tests in a particular study area and remain mechanistically interpretable. The key ingredients in our case are (1) a diverse biological data set, including not just synoptic observations of nutrients and chlorophyll, but also in situ process studies examining phytoplankton growth and microzooplankton grazing, and (2) approaching the problem of choosing free parameters as an empirical problem in quantitative ecology, not a problem in statistics or optimization. The result is a model that captures not just the distribution of nutrient and biomass stocks within our study area, but also essential community rates.

[9] In the next section we describe the model formulation, including our empirical methods for choosing vital rates for phytoplankton and zooplankton. In section 3 we compare a model hindcast of July 2004 with observations. In section 4 we compare results when the Columbia River is and is not included, in order to quantify the effect of plume dynamics on regional primary production.

2. Model Formulation

2.1. Circulation Model

[10] *MacCready et al.* [2009] describe the circulation model used in this study in detail. The model is implemented using Regional Ocean Modeling System (ROMS), Rutgers version 2.2 [*Haidvogel et al.*, 2000]. The model uses a finite difference scheme in the horizontal and a generalized, irregularly spaced S-coordinate in the vertical. Our implementation has 20 depth levels. The turbulence closure is Generic Length Scale [*Umlauf and Burchard*, 2003] with Canuto A stability functions [*Canuto et al.*, 2001]. The model domain is shown in Figure 1. Horizontal resolution is $\sim$500 m at the mouth of the Columbia, telescoping out to $\sim$7 km at the northwestern and southwestern corners. The Columbia River beyond a point 50 km upstream of the mouth is replaced by a straight 3 km wide, 3 m deep channel, to allow tidal energy to propagate freely past the estuary. Grays Harbor and Willapa Bay are both included as riverless embayments (Figure 1). The baroclinic time step, which is also the time step for the ecosystem model, is 51.75 s.

[11] A three-month hindcast of June–August 2004 was performed, using time-varying atmospheric forcing, variable river flow, and tides. Hourly wind and atmospheric forcing is taken from the 4 km Northwest Modeling Consortium MM5 regional forecast model [*Mass et al.*, 2003]; daily Columbia river flow is taken from USGS gauge 14246900 at Beaver Army Station (http://waterdata.usgs.gov/or/nwis/); and ten tidal constituents from the TPXO6 analysis [*Egbert et al.*, 1994; *Egbert and Erofeeva*, 2002] are applied as surface height and depth-averaged velocity boundary conditions. Boundary conditions for tracers, subtidal velocity, and subtidal surface height come from the Navy Coastal Ocean Model (NCOM), California Current System [*Barron et al.*, 2006; *Kara et al.*, 2006]. The first month of this three-month hindcast is treated as spin-up.

[12] *Liu et al.* [2009] describes a comprehensive skill assessment of this hindcast, in which Willmott skill scores [*Willmott*, 1981] were determined separately for three dynamical zones (estuary, near-field plume, and far-field plume), surface and deep layers, and tidal and subtidal timescales, for several variables (velocity, temperature, salinity, and sea level). The Willmott skill is defined as

$$WS = 1 - \frac{\left\langle (m-o)^2 \right\rangle}{\left\langle \left(|m - \langle o \rangle| + |o - \langle o \rangle| \right)^2 \right\rangle} \tag{1}$$

where m and o are model and observations. $WS = 1$ indicates a perfect model, and $WS = 0$ indicates a model whose predictive power is equivalent to taking the mean of the data. The average of all skill scores is 0.65. In general, model skill is higher in the Columbia estuary and top 20 m than deeper in offshore waters.

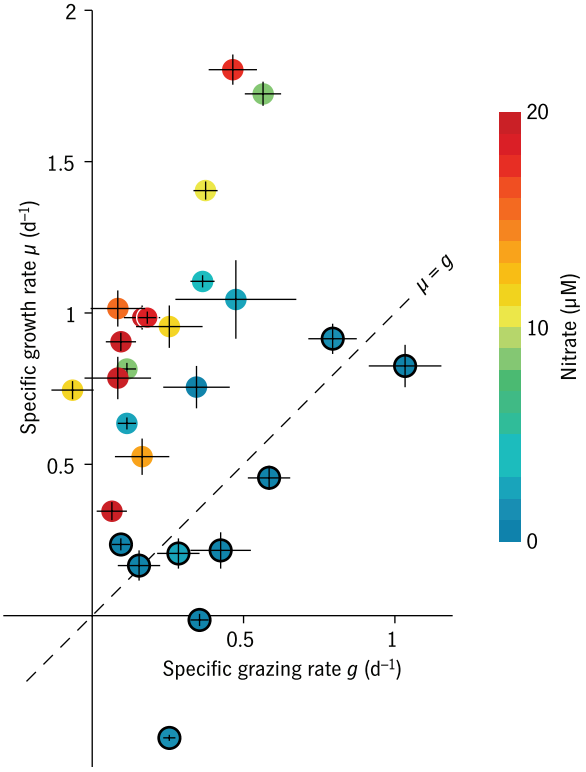

Figure 2. Overview of results from dilution experiments used in this study. Each point represents one experiment. Low-nutrient, near-equilibrium points used to diagnose zooplankton rate parameters are marked with black circles. Standard errors are indicated with vertical and horizontal bars.

2.2. Dilution Experiments and Other Observations

[13] Before describing the ecosystem model, we need to describe the biological observations that motivate it. The data we use for model calibration and validation comes from two three-week cruises (RISE1 and RISE3) aboard the R/V *Wecoma* in July 2004 and August 2005. Both cruise periods were upwelling dominated, although intervals of weak and downwelling-favorable wind occurred during both as well. We make particular use of conductivity-temperature-depth (CTD) data from July 2004 (see section 3), and microzooplankton dilution experiments from both cruises. Since the dilution experiment data are crucial to our treatment of zooplankton in the model and choice of vital rate parameters, we will describe them here in some detail.

[14] The dilution method [*Landry and Hassett*, 1982] is used to determine the impact of microzooplankton grazing on natural phytoplankton communities. In this method, the density of the grazers, and thus grazing pressure, is manipulated by dilution with filtered seawater, and the net growth of the phytoplankton community (as measured by chlorophyll changes) over 24 h is measured in a dilution series. Phytoplankton intrinsic growth rate is assumed to remain the same in all dilutions. A linear regression model can be fit relating net growth to dilution level, and growth rate μ of the phytoplankton is determined from the y-intercept and grazing rate g from the slope. In the experiments reported here, treatments were amended with nutrients to prevent nutrient limitation during incubation; the in situ phytoplankton growth rate μ was estimated from the sum of the net growth in undiluted control samples without added nutrients and the estimated grazing rate [*Olson et al.*, 2008]. Each experiment yields a phytoplankton community growth rate μ and a community grazing rate g such that

$$\frac{\partial P}{\partial t} = (\mu - g)P \tag{2}$$

where P is phytoplankton biomass and t is time. All experiments used here are from seawater collected at a depth corresponding to 50% surface irradiance, usually 2–3 m depth; water temperature of these samples ranged from 9.6 to 16.3°C. Results are summarized in Figure 2. At high nitrate levels (i.e., in recently upwelled water), phytoplankton growth far exceeds grazing. When nitrate is depleted, μ and g are comparable, indicating a phytoplankton population near equilibrium and sometimes even declining (when $\mu < g$).

[15] Note that mesozooplankton were excluded by filtering samples through 200 μm mesh, so g represents the grazing impact of microzooplankton, not copepods or other mesozooplankton. Copepod grazing experiments from 2003 in northern Washington waters [*Olson et al.*, 2006] suggest that in this region (like many others [*Calbet and Landry*, 2004]) microzooplankton have a far greater grazing impact on the phytoplankton community than do copepods. Copepods in fact select for microzooplankton prey [*Leising et al.*, 2005; *Olson et al.*, 2006] and thus may even have a positive effect on phytoplankton biomass via a trophic cascade [*Olson et al.*, 2006].

[16] Cell counts for both phytoplankton and microzooplankton were also obtained for each dilution experiment. Picoplankton, small flagellates and dinoflagellates were counted from gluteraldehyde-preserved samples filtered onto 0.2 or 0.8 μm membrane filters using epifluorescent microscopy [*Lessard and Murrell*, 1996], while ciliates, larger dinoflagellates, and diatoms were counted in settled Lugol's solution–preserved samples with an inverted Zeiss microscope. Autotrophs and heterotrophs were distinguished by taxa or autofluorescence. Picoplankton were sized using digital images and image analysis software; other cells were sized using a computer-aided digitizing system [*Roff and Hopcroft*, 1986]. C biomass was estimated from cell volumes using the equations of *Menden-Deuer and Lessard* [2000] for diatoms, nanoflagellates and dinoflagellates, *Worden et al.* [2004] for picoplankton, and *Putt and Stoecker* [1989] for ciliates. In July 2004 and August 2005, diatoms dominated the phytoplankton biomass, although photosynthetic dinoflagellates (mainly *Prorocentrum*) were abundant as well [*Frame and Lessard*, 2009]. Heterotrophic dinoflagellates usually dominated the microzooplankton biomass during both cruises, although in August, mixotrophic and heterotrophic ciliates dominated at times.

[17] Thus a logical, minimal set of components for an ecosystem model intended to match these observations and reproduce Figure 2 numerically would be (1) a finite pool of available nitrate, (2) a population of diatoms, and (3) a population of microzooplankton, subject to grazing by

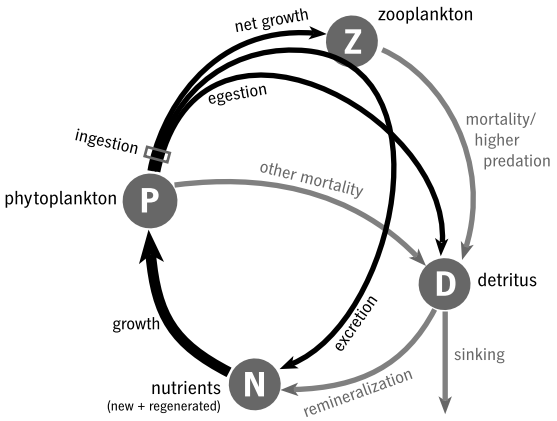

Figure 3. Schematic of the ecosystem model.

unobserved copepods. The implementation of this model is described in the next section.

2.3. Ecosystem Model Design

[18] Our ecosystem model is a budget that tracks nitrogen in every grid cell of the circulation model, in four phases: dissolved nutrients (N), phytoplankton (P), zooplankton (Z), and detritus (D). We track nitrogen alone because it is almost always the limiting nutrient in this system: silica and iron appear not to be limiting in Columbia River plume–influenced waters [*Bruland et al.*, 2008]. The model uses the fasham.h module included in ROMS as a framework (input/output, time stepping, and the calculation of detrital sinking are retained) but the stock-flux network and functional forms for biological fluxes are rewritten to suit our study area and questions. The model equations are as follows:

$$\frac{\partial P}{\partial t} = \mu_i(E,N)P - I(P)Z - mP + advection + diffusion \quad (3a)$$

$$\frac{\partial Z}{\partial t} = \varepsilon I(P)Z - \xi Z^2 + advection + diffusion \quad (3b)$$

$$\frac{\partial D}{\partial t} = (1-\varepsilon) f_{egest} I(P)Z + mP + \xi Z^2 - rD - sinking + advection + diffusion \quad (3c)$$

$$\frac{\partial N}{\partial t} = -\mu_i(E,N)P + (1-\varepsilon)\left(1 - f_{egest}\right)I(P)Z + rD + advection + diffusion \quad (3d)$$

[19] See also the schematic in Figure 3. Definitions and units for all free parameters are given in Table 1; further explanations follow.

[20] The instantaneous phytoplankton growth rate $\mu_i(E, N)$ depends on light E and nutrient concentration N as

$$\mu_i(E,N) = \mu_0 \frac{N}{k_s + N} \frac{\alpha E}{\sqrt{\mu_0^2 + \alpha^2 E^2}} \quad (4)$$

where μ_0 is the maximum instantaneous growth rate (when neither nutrients nor light is limiting), k_s is the half-saturation for nutrient uptake, and α is the initial slope of the growth-irradiance curve. E is photosynthetically available radiation (PAR) at a given depth z:

$$E(z) = E_{surface} \exp\left(att_{sw}\, z + att_P \int_z^{surface} P(z')dz' \right) \quad (5)$$

where att_{sw} and att_P are light attenuation coefficients for seawater and phytoplankton: the integral term in (5) expresses phytoplankton self-shading. This model assumes, as is common for NPZ-type models, that nutrient uptake and phytoplankton growth are simultaneous and equivalent. Note also that we have combined nitrate, ammonium, and other forms of dissolved nitrogen into a single N pool for the sake of parsimony: kinetics experiments [*Kudela and Peterson*, 2009] suggest that the error thus introduced into the nutrient limitation term is minor (10% or less) in the high-productivity waters we are interested in. (If we were more interested in the oligotrophic waters seaward of the upwelling zone, the details of ammonium uptake and regeneration would be far more important.) For simplicity we will sometimes refer to the model N pool as "nitrate" to distinguish it from "total nitrogen" ($N + P + Z + D$) or nitrogen in other phases (P, Z, D).

[21] Zooplankton ingestion $I(P)$ depends on prey concentration P as

$$I(P) = I_0 \frac{P^2}{K_s^2 + P^2} \quad (6)$$

where I_0 is the maximum ingestion rate and K_s is a half-saturation coefficient. We have used a quadratic prey saturation response [*Fulton et al.*, 2003] because this functional form provides a partial refuge from grazing when $P \ll K_s$. This damps the boom-and-bust of predator-prey cycles much as (we conjecture) natural diversity in vital rates and species-specific interactions does in reality. The total grazing flux $I(P)$ Z is partitioned into excretion (a flux from P to N, via Z), egestion (a flux from P to D), and zooplankton net growth (a flux from P to Z) using two parameters, ε and f_{egest}.

[22] Since we do (unlike some NPZ studies) explicitly include the day-night cycle in our PAR forcing fields, the 24 h average growth rate μ that the dilution experiments yield and the instantaneous growth rate μ_i are not identical. The relationship between these rates is approximately

$$\mu = \frac{14\ h}{24\ h} \mu_{i\ at\ noon} \quad (7)$$

where 14 h is the July photoperiod at our latitude. The specific grazing rate g that the dilution experiments yield is related to the ingestion term, definitionally, by

$$g\ P \equiv I(P)Z \quad (8)$$

[23] A small mortality loss mP is imposed on phytoplankton in addition to zooplankton grazing, as is common [e.g.,

Table 1. Free Parameters Used in the Ecosystem Model, Values Chosen, and Sources for Those Values

	Description	Value	Standard Deviation	RISE Observations	General Lab Studies	A Priori	Source
			Phytoplankton Parameters				
μ_0	maximum instantaneous growth rate	2.2 d^{-1}	0.9	yes			dilution experiments at high nutrient levels (n = 13)
att_{sw}	light attenuation by seawater	0.13 m^{-1}	0.06	yes			2004 CTDs (n = 15)
att_P	light attenuation by phytoplankton	0.018 m^{-1} $(\mu M\ N)^{-1}$	0.008	yes			2004 CTDs (n = 15)
α	initial slope of growth-light curve	0.07 $(W\ m^{-2})^{-1}$ d^{-1}	0.06	yes			photosynthesis-irradiance curves from deckboard incubations, 2004–2006 (n = 55)
k_s	half-saturation for nitrate uptake	4.6 μM N	1	yes			deckboard kinetics experiments, 2005 (n = 3) [see *Kudela and Peterson*, 2009]
m	nongrazing mortality	0.1 d^{-1}				yes	
chl:N	chlorophyll: nitrogen ratio	2.5 mg chl $(mmol\ N)^{-1}$	3.3	yes			CTDs 2004–2005 (n = 121)
			Zooplankton Parameters				
I_0	maximum ingestion rate	4.8 d^{-1}	8.5	yes			dilution experiments near growth-grazing equilibrium (n = 9)
ξ	mortality	2.0 d^{-1} $(\mu M\ N)^{-1}$	3.9	yes			dilution experiments near growth-grazing equilibrium (n = 9)
K_s	half-saturation for ingestion	3 μM N			yes		average for ~60 microzooplankton and mesozooplankton spp. [*Hansen et al.*, 1997]
ε	gross growth efficiency	0.3			yes		average for ~60 microzooplankton and mesozooplankton spp. [*Hansen et al.*, 1997]
f_{egest}	fraction of losses egested	0.5				yes	
			Detritus Parameters				
r	remineralization rate	0.1 d^{-1}				yes	
w_{sink}	sinking rate	8 m d^{-1}				yes	

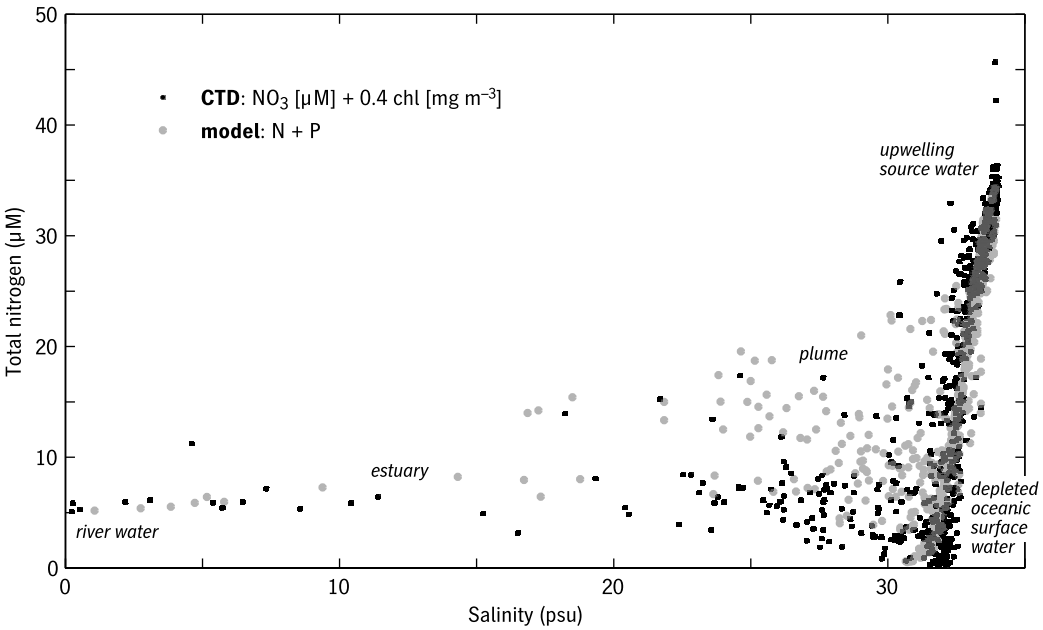

Figure 4. Total nitrogen as a function of salinity from July 2004 CTDs and the model at corresponding locations and times. Total nitrogen is estimated from CTD data as nitrate plus chlorophyll times a conversion factor (see Table 1).

Fennel et al., 2001; *Spitz et al.*, 2005; *Botsford et al.*, 2006]. This term is mathematically equivalent to the way coagulation of diatoms is often included in NPZ models as well. In (7) and (8) we have assumed that $m \ll \mu, g$ in order to harmonize (2) and (3a); comparing our value for m, 0.1 d^{-1}, with the empirical rates in Figure 2 shows that in practice, mortality is consistently secondary to grazing but not actually negligible. The mortality imposed on zooplankton (ξZ^2) is more important dynamically. Since Z represents microzooplankton in our model, this mortality term largely represents predation by copepods and euphausiids. Writing this higher predation term as quadratic in Z rather than linear [*Steele and Henderson*, 1992; *Edwards and Yool*, 2000] implicitly assumes that predator biomass is proportional to Z rather than isotropic; both options are meager representations of copepod ecology and neither seems to us a better or worse assumption a priori. Mathematically speaking the quadratic closure, like the quadratic grazing term described previously, helps moderate booms and busts we believe are artificial.

[24] Finally, there are two losses from the detrital pool, remineralization (to N) at a rate r, and vertical sinking at a velocity w_{sink}. Detrital dynamics are the most speculative aspect of this model, as in many NPZ-type models. The D pool should be thought of very generically, perhaps as "storage" rather than "detritus," since really it represents all forms of nitrogen that are neither phytoplankton/microzooplankton biomass nor dissolved and available for uptake: that is, not just detritus but copepods, salmon, cormorants, etc. Including a D pool prevents artificially dense accumulations of Z offshore [see *Spitz et al.*, 2003].

2.4. Boundary Conditions

[25] Boundary and initial conditions have deliberately been kept very simple: this makes our model much more easily interpretable in mechanistic terms, although less useful as a simulation of chlorophyll biomass in the far field. Only seed stocks (0.01 μM N) of P and Z are introduced at ocean and river boundaries. The river source carries 5 μM N, in accordance with summer 2004 observations (see Figure 4 below). A spatially variable but temporally constant N field is introduced at the ocean boundaries. We found, as did *Spitz et al.* [2003], that model results are sensitive to the vertical profile of total nitrogen introduced in initial and boundary conditions, which in our case is represented by N alone. To choose this profile, we constructed a piecewise linear nitrate-salinity curve for all July 2004 CTDs, from (S, N) = (31.9 practical salinity units, 0 μM) to (32.75, 21.4) to (34.6, 41), and applied it to the time mean salinity boundary conditions from NCOM. The point-by-point validation against CTD salinity and nitrate measurements (Figure 4) provides a consistency check on this method. Initial conditions are a simple interpolation of the initial boundary conditions; the first month of simulation is treated as spin-up and ignored for the biological results as for the physics.

[26] More complex boundary conditions are certainly possible: we could have let nitrate at the boundaries vary in time, or run the model to equilibrium under climatological winds and used the resulting N, P, Z, and D fields. However, this is a highly advective system; under moderate upwelling, water from the northern boundary traverses the entire domain in only 10 days [*Banas et al.*, 2009], and if the boundary inputs are not kept trivially simple, it becomes very difficult to distinguish event-scale processes within the domain from event-scale variations in imposed boundary conditions advecting through. Our choice of boundary conditions is equivalent to isolating the biology of this along-coast reach from its neighbors, so that all biomass seen in the model can be attributed to primary production and grazing within the study area itself.

Table 2. Sensitivity of a One-Dimensional Version of the Model to Parameter Changes[a]

	Surface chl		Primary Production, 0–30 m		Nutrient Limitation $N/(k_s + N)$		Grazing Limitation g/μ	
	Halved	Doubled	Halved	Doubled	Halved	Doubled	Halved	Doubled
				Nutrient Supply				
N_0	**−53**	**190**	**−56**	**81**	−22	22	**−35**	−17
				Phytoplankton Parameters				
μ_0	4	−1	8	2	**160**	**−42**	−7	−3
att_{sw}	−9	22	−7	−13	−2	10	−10	12
att_P	−8	17	−9	−5	−1	5	−10	12
α	12	−8	−2	−5	7	−3	8	−8
k_s	−1	2	0	−1	8	−11	−2	2
m	23	−27	5	−7	−2	6	8	−17
				Zooplankton Parameters				
I_0	**71**	**−54**	−20	9	−9	**110**	**−73**	**170**
ξ	**−30**	**37**	4	−9	10	−5	**48**	**−42**
K_s	−24	**35**	3	−11	20	−7	**86**	**−52**
ε	**50**	**−47**	−5	−14	−4	3	1	−27
f_{egest}	19	−25	20	−29	6	−9	**40**	**−64**
				Detritus Parameters				
r	−4	8	−8	14	−1	2	−4	7
w_{sink}	7	−4	13	−8	3	−1	8	−4

[a]A 30 m water column was initialized with a pulse of nutrients (N_0, 20 μM N in the base case) and allowed to evolve under steady light for 20 days. Values shown are percent changes in four metrics (surface chlorophyll, gross primary production (i.e., nutrient uptake) vertically integrated to 30 m, measures of nutrient limitation, and measures of grazing limitation) in response to twofold changes (halving and doubling) in each parameter. All metrics are means over 20 days. Parameters are identified in Table 1. Changes greater than ±30% are shown in bold.

2.5. Parameters and Sensitivity

[27] Sources for values of all model parameters are given in Table 1. Parameters chosen on the basis of data from RISE cruises are labeled "RISE Observations" The determination of three of these (μ_0, I_0, and ξ) is indirect and is discussed further in section 2.6 below. Two parameters labeled "general lab studies" (ε and K_s) were chosen using average values from the comprehensive review by *Hansen et al.* [1997]: they find K_s to be highly variable (hundredfold differences) among grazer species but ε relatively consistent on this broad scale. Remaining parameters chosen simply in accordance with NPZ modeling tradition (for lack of a better option) are labeled "a priori."

[28] Results of a sensitivity analysis in a simplified domain are shown in Table 2. A one-dimensional water column, with mixing and sinking but no other physics, was initialized with a uniform pulse of nutrients (20 μM, in the base case) and allowed to evolve for 20 days under constant light. This scenario is intended to represent a profile through the oceanic surface layer during an idealized upwelling period, following a water parcel as it moves south and offshore from the inner shelf upwelling zone, similar to the zero-dimensional "mixed layer conveyor" used by *Botsford et al.* [2006]. Four metrics were calculated: mean surface chlorophyll, total primary production (integrated in both depth and time), the nutrient limitation factor $N/(k_s + N)$ (see equation (4)) and g/μ, a measure of grazing limitation or trophic transfer, discussed further in section 4.1. Table 2 gives the percent change in each metric for a halving and a doubling of each model parameter, and for a halving and doubling of the initial nutrient concentration N_0.

[29] As expected, phytoplankton biomass and production are highly dependent upon nutrient availability. Integrated primary production is not sensitive to any other parameter, implying that over 20 days and 30 m we mostly average over the variations in depth and timing associated with the model's biological dynamics, so that what remains is the effect of total available nutrient "fuel." This insensitivity might not occur in a system less strongly forced by nutrient supply. Note that the response of integrated primary production to μ_0 and the light parameters is nonmonotonic, with changes of the same sign in response to both halving and doubling the parameter. This suggests a complex dependence beyond the scope of this simple sensitivity analysis. Mean chlorophyll and grazing limitation are likewise relatively insensitive to the phytoplankton growth parameters, but they are in fact sensitive to the grazing parameters, particularly the maximum ingestion rate I_0, discussed further in the next section. Finally, this analysis provides reassurance that our results are not sensitive to the a priori parameters (see Table 1) describing detrital processes (r, w_{sink}) or phytoplankton "other mortality" m.

2.6. Choice of Rate Parameters

[30] The scale for the vital rates μ and g is set by three parameters, μ_0, I_0, and ξ. We chose these parameters as follows. To estimate μ_0 (the instantaneous growth rate without nutrient limitation) from measurements of μ (the 24 h average rate, with varying levels of nutrient limitation), we took the subset of μ data for which measured $[NO_3] > k_s$ and applied nutrient limitation and photoperiod corrections:

$$\mu_0 \sim \frac{24\ h}{14\ h}\ \frac{k_s + [NO_3]}{[NO_3]}\mu \tag{9}$$

[31] This yields $\mu_0 = 2.2 \pm 0.9\ d^{-1}$ (n = 13), consistent with the diatom growth rates reported by *Tang* [1995]. To estimate I_0 and ξ, we took the subset of dilution experiments representing far-field, nutrient-depleted, near-equilibrium populations (those for which $[NO_3] < k_s$ and $\mu - g <$

0.3 d^{-1} (see Figure 2)) and used μ, g, P, and Z from these experiments to evaluate the equilibrium solution of the model equations. Advection and diffusion were neglected, such that this solution represents a community equilibrium following a water parcel. If we assume that the zooplankton community adapts so as not to be prey limited in its equilibrium state, then by (8),

$$g_{eq} P_{eq} \sim I_0 Z_{eq} \tag{10}$$

where *eq* denotes equilibrium values. For consistency with the rest of the model analysis, P_{eq} (in nitrogen units) was estimated from chlorophyll (chl) data using a chl:N ratio of 2.5 mg $mmol^{-1}$. This chl:N ratio was calculated from mean chl:C and C:N ratios from 121 CTD casts, 2004–2005 (see Table 1). Instead of assuming the same C:N ratio for zooplankton, we estimated Z_{eq} from carbon biomass assuming a Redfield C:N ratio: it is frequently observed that microzooplankton have a C:N ratio near Redfield or lower even when the phytoplankton C:N ratio is much higher [*Stoecker and Capuzzo*, 1990].

[32] Solving (9) for I_0 yields the estimate 4.8 ± 8.5 d^{-1}. This is, clearly, not a tightly constrained value, but the central value of 4.8 d^{-1} is 5–10 times higher than the ingestion rates assumed by several other recent Northeast Pacific NPZ modeling studies with a single Z compartment [*Denman and Peña*, 1999; *Batchelder et al.*, 2002; *Spitz et al.*, 2005; *Botsford et al.*, 2006], although similar to the rate chosen by *Edwards et al.* [2000] and others to represent microzooplankton. For comparison, the review by *Hansen et al.* [1997] reports a range of herbivorous dinoflagellate and ciliate ingestion rates from 0.24 to 11.54 d^{-1} (n = 21, mean ± std dev 4.0 ± 2.8 d^{-1}). That our central value for I_0 is well within this range is a consistency check on the organismal interpretation of our model. The huge variance in empirical rates also supports our supposition that the first-order uncertainty in our I_0 estimation primarily reflects real planktonic diversity, rather than being a statistical problem. The relative uncertainty does not improve (and the I_0 estimate does not change significantly) if we repeat the estimation from (10) using all the data, or only the high phytoplankton biomass data, instead of the near-equilibrium subset.

[33] We can in fact estimate the zooplankton mortality parameter ξ from experimental data as well. Combining (9) with the equilibrium solution to the zooplankton equation (3b) yields

$$\varepsilon g_{eq} P_{eq} \sim \xi Z_{eq}^2 \tag{11}$$

[34] Solving this for ξ yields the estimate 2.0 ± 3.9 d^{-1} $(\mu M\ N)^{-1}$; the equivalent linear mortality rate $\xi Z_{eq} \sim 1.5\ d^{-1}$. This is the rate of predation on microzooplankton (by copepods, say) required to balance the grazing by microzooplankton observed in low-nutrient, far-field conditions. This rate is, again, not well constrained, but it is much higher than what one might assume a priori: *Spitz et al.* [2005], for example, use a combined excretion and mortality rate of 0.3 d^{-1}.

[35] To summarize: we have tuned the controlling rate parameters in the model to match a subset of the observations. Phytoplankton growth has been tuned to match maximum rates in the nutrient-replete upwelling zone. Zooplankton ingestion and mortality have been tuned to match stocks and rates in nutrient-depleted offshore waters. The tuned rate parameters are sensible and interpretable in organismal terms. Since we used only a subset of the data to choose these parameters, the spatial variability in modeled stocks and rates remains a noncircular validation test. In the next section we test these spatial patterns against CTD, satellite, and dilution experiment data.

3. Model Validation

3.1. Total Nitrogen

[36] The first model validation required is a verification that the total biologically available nitrogen in the model is not biased by poor boundary conditions or poor upwelling dynamics. In Figure 4, total nitrogen from the model and matching estimates from CTD data are shown for every CTD bottle sample of nitrate taken between 45.5°N and 47°N during July 2004. Total nitrogen is estimated from CTD data as nitrate concentration plus chlorophyll concentration times the mean observed phytoplankton N:chl ratio (Table 1). For consistency, model total nitrogen is calculated as $N + P$ instead of $N + P + Z + D$ (the choice makes no difference in the interpretation of results). In both model and observations, the water sampled spans a triangular area in this mixing diagram, with the river end-member, upwelling source water, and depleted, far-field oceanic surface water defining the three corners. This mixing diagram is similar to that shown by *Lohan and Bruland* [2006]. In the plume (salinities ~24–31), model samples are biased toward higher total nitrogen values than observations, but the envelopes of model and CTD data in the plume match well, indicating that Columbia estuary water is mixing with ocean water of approximately the correct salinity and nutrient content. In fact, a more refined approach to estimating the phytoplankton nitrogen contribution from CTD data would probably improve agreement in the plume, since cells in nutrient-rich, turbid plume water are likely to have higher chl:N ratios than the average over all data used here.

[37] The mixing diagram in Figure 4 verifies the range of water masses seen in the study area but not their spatial distribution. Model skill at point-by-point reproduction of the salinity, nutrient, and biomass distributions shown in Figure 4 is quantified in Table 3. Willmott skill scores for nitrate and chlorophyll are 0.92 and 0.77 for the data set as a whole and 0.82 and 0.64 for the top 20 m alone. Much of this skill probably indicates a generally correct reproduction of depth variation and gross upwelling-downwelling variations in nutrient supply to the surface layer. To evaluate model performance and modes of error more mechanistically, in the next section and Figures 5, 6, and 7, we describe spatial patterns of nutrients and phytoplankton during a sustained upwelling event in late July 2004.

3.2. Nutrients and Chlorophyll

[38] Cross-shelf sections of model nutrients (N) off both Washington and Oregon are compared with matching CTD nitrate sections in Figure 5. For temporal context, see the wind time series in Figure 7 below. Solid contours are shown every 5 μM, but shading and dashed contours every

Table 3. Model Performance in Point-by-Point Comparisons With CTD Data at All Times and Depths Where Nutrient Bottle Samples Were Collected[a]

	All Data			Top 20 m		
	Correlation Coefficient	Relative Error (%)	Willmott Skill	Correlation Coefficient	Relative Error (%)	Willmott Skill
Salinity	0.81	3	0.89	0.78	5	0.87
Nitrate	0.87	32	0.92	0.71	69	0.82
Chlorophyll	0.62	62	0.77	0.41	60	0.64
Total nitrogen $N + P$	0.86	28	0.91	0.73	49	0.83

[a]The data used are the same as those shown in Figure 4. Correlation coefficient, relative error (i.e., $\langle|\text{measured} - \text{observed}|\rangle/\langle\text{observed}\rangle$), and Willmott skill score (equation (1) above) are given for each variable, for the data set as a whole ($N = 417$), and for the top 20 m only ($N = 376$).

1 μM are used to highlight the subrange in which nutrient limitation occurs: at concentrations of $k_s = 4.6$ μM, primary production is reduced by half (equation (4)). The model reproduces several key features well. The outcropping of high-nitrate water off Oregon (45.5°N) (Figures 5c and 5d) has the right spatial scale (20 km), and the much weaker outcropping off Washington (47°N) (Figures 5a and 5b) is captured as well. The depth of the nutricline (~20 m) is correct off Oregon, and correct off Washington out to approximately 35 km from the coast, although subsurface nutrients farther offshore (on the outer shelf and slope) are under-represented. Note that offshore surface values are not directly comparable: surface nitrate is <1 μM over large areas in the CTD data and corresponding model nutrient levels are 1–2 μM, but this is likely to be a matter of definitions (nitrate alone in the CTD data, total dissolved nutrients in the model), rather than simply a dynamical error.

[39] The model's reproduction of the depth and outcropping of the nutricline suggests that the balance of upwelling and biological drawdown in the model is qualitatively correct. Validation against chlorophyll data is equally encouraging. Surface and integrated chlorophyll during the same upwelling event are shown in Figures 6 and 7. Comparison with a Sea-viewing Wide Field-of-view Sensor image from 23 July (Figure 6) shows that the model correctly reproduces a number of mesoscale features during this event (features described in more detail by *Banas et al.* [2009]; see Figure 3

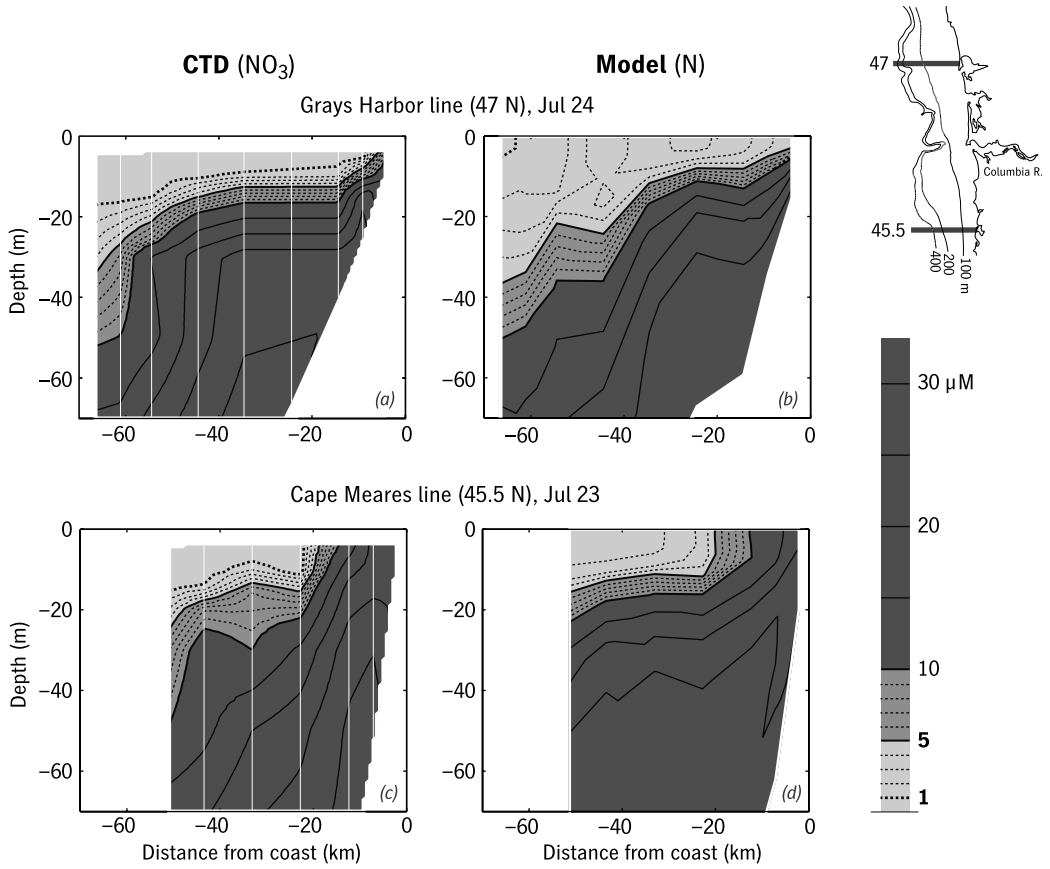

Figure 5. Comparison between nitrate from (a, c) cross-shelf CTD sections and (b, d) corresponding sections of model nutrients, during the same sustained upwelling event depicted in Figures 6 and 7. Solid contours appear every 5 μM N, and dashed contours appear every 1 μM between 0 and 10 μM. The locations of CTD casts (Figures 5a and 5c) are marked with white lines.

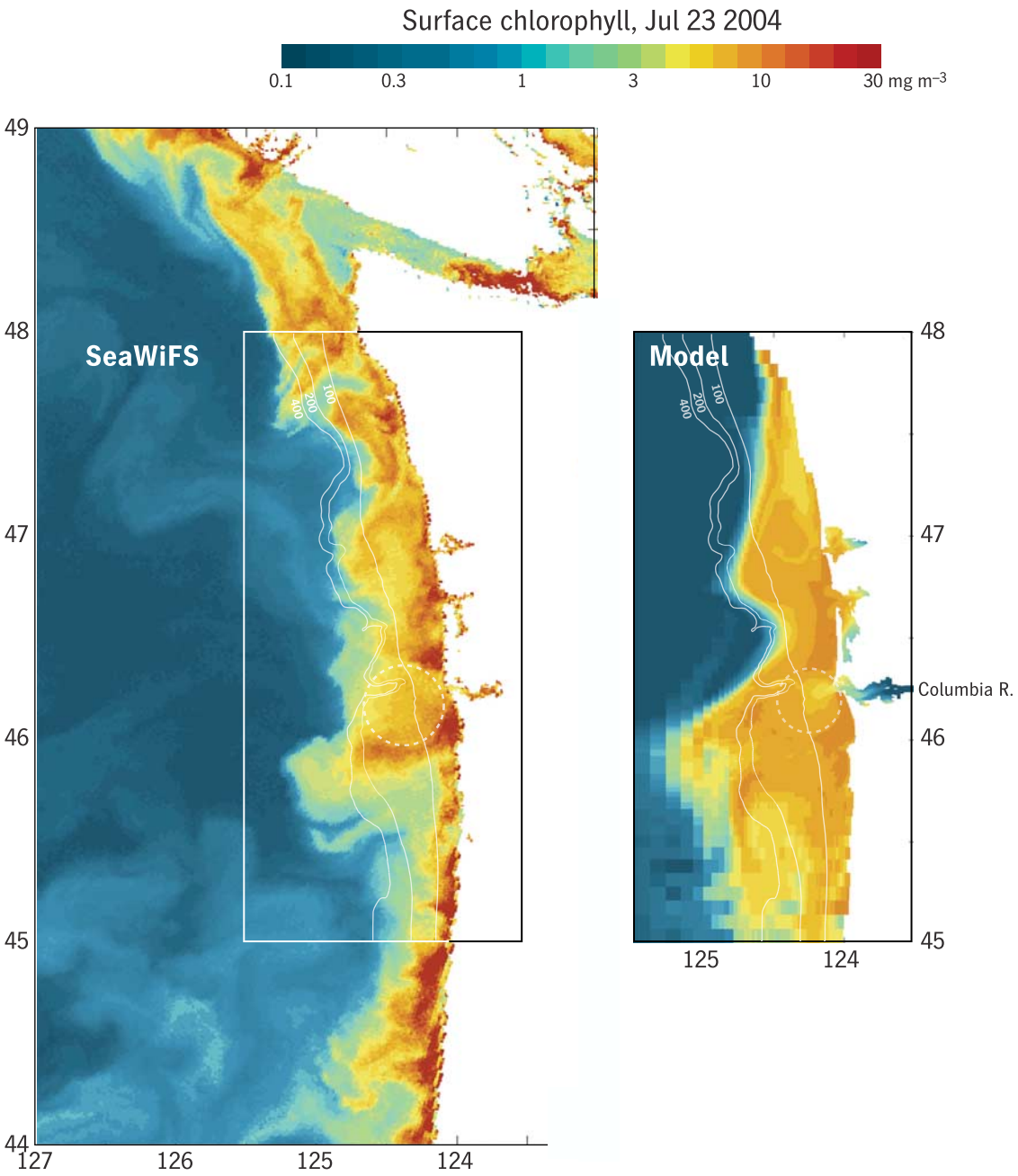

Figure 6. Model chlorophyll at the surface compared with chlorophyll from Sea-viewing Wide Field-of-view Sensor (SeaWiFS), 23 July 2004, at the beginning of a sustained upwelling event. The 100 m, 200 m, and 400 m isobaths are marked. Dashed circles indicate relative lows in chlorophyll in the vicinity of the near-field plume.

in that study). There is a local maximum in biomass on the outer shelf near 47°N, associated with a transient topographic eddy caused by the variation in shelf width there. A bloom extends beyond the slope into the deep ocean near 46°N, in the far-field Columbia plume. There is high inner shelf biomass immediately south of the river mouth (~46°N) and north of the river mouth to ~47°N, with a local minimum in surface chlorophyll in the near-field plume (dashed white circles). One discrepancy, caused by our choice of boundary conditions (nutrients but no biomass, only seed stock; section 2.4 above), is an unrealistic lack of biomass offshore in the northern part of the domain. This discrepancy is a useful indicator of the dividing line between the region controlled by biological dynamics within the domain and the region controlled by advection from farther north. Reassuringly, it coincides with where one would place this dividing line on the basis of three-dimensional particle tracking [see *Banas et al.*, 2009, Figure 3].

[40] The absolute magnitude of surface chlorophyll is more variable in reality than in the model results: the inner shelf highs are higher and the outer shelf lows are lower, by approximately a factor of two. This bias is reduced when we compare vertically integrated chlorophyll with CTD data

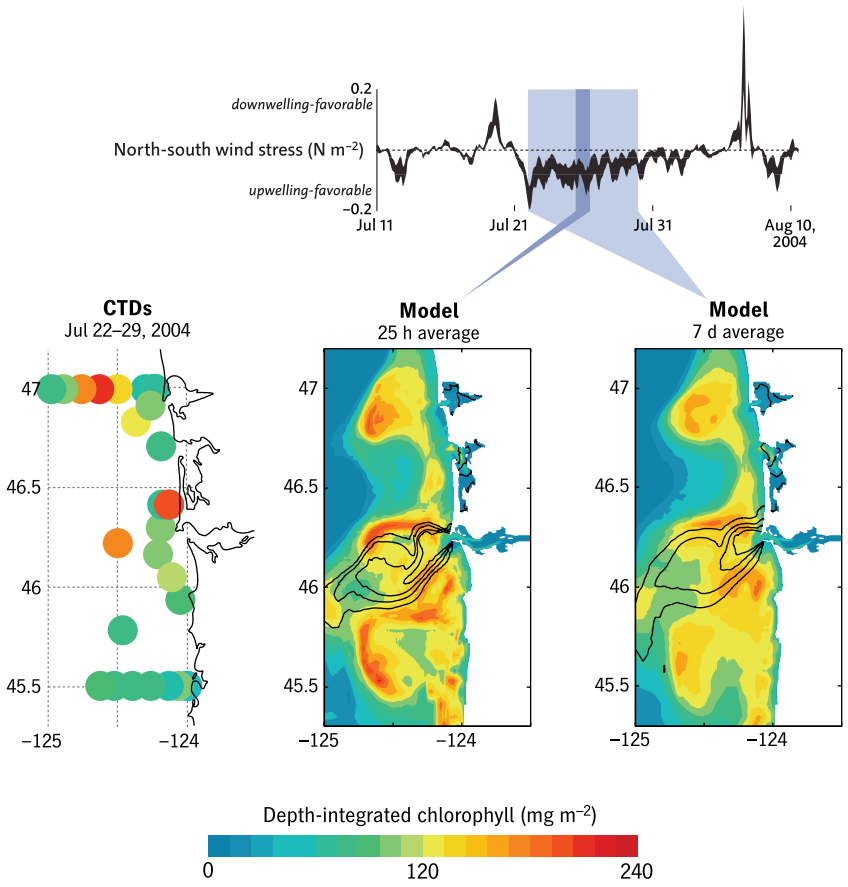

Figure 7. Depth-integrated chlorophyll from CTDs 22–29 July (over the course of a sustained upwelling event), from a tidal (25 h) average in the model on the middle day of that time period, and from an average of model fields over the entire 7 days. Surface salinity contours (24, 26, 28, and 30 practical salinity units (psu)) are shown in black to indicate the location of the Columbia River plume.

(Figure 7) rather than looking only at the surface field. CTD data (fluorometer chlorophyll, integrated to the bottom) over 7 days of upwelling (22–27 July 2004) have been conflated in order to highlight the spatial pattern of phytoplankton biomass. The corresponding model field is shown for the middle 25 h of this time period and also for an average over the full 7 days: comparing these two model fields suggests that temporal aliasing might cause ~30% errors when we conflate observations scattered over these 7 days.

[41] The point-by-point model-data comparison is no better on average than the surface-field comparison in Figure 6 (relative error ~50%), but if we allow for some spatial displacement of transient features, the comparison is very accurate in most of the domain. Integrated chlorophyll in the nearshore of both Washington and Oregon is 60–100 mg m^{-2}, in both model and observations. Along 47°N there is an outer shelf high, ~30 km wide, with integrated chlorophyll up to ~200 mg m^{-2}. Similar values are seen along the northern edge of the plume but not in the plume. The model shows a narrow band of high biomass along the southern edge of the plume, like that along the northern edge, but this was apparently under-sampled in the CTD data set (it is present in the 23 July satellite image shown in Figure 5.) There is also, more dubiously, a large patch of high biomass offshore of Oregon in the model that observations do not show. This patch corresponds to a cyclonic recirculation that *Banas et al.* [2009] hypothesized was an artifact of the southern and western boundary conditions: a region of erroneously high retention, not necessarily an error in the biological dynamics.

3.3. Growth and Grazing

[42] As discussed above, nutrient and chlorophyll fields are not by themselves comprehensive or mechanistic tests of an ecosystem model. In Figure 8, we show simultaneous validation of N, P, Z, μ, and g against dilution experiment data, i.e., every model element except for the regeneration pathways (Figure 3). Since we have only simulated one of the two cruise periods from which dilution data are taken (and since we would not expect the model to have much point-by-point predictive power in patchy, transient fields anyway) we have arranged the data into a summary profile along the plume axis under upwelling conditions. Model stocks and rates are shown along the centerline of the plume, averaged over the top 5 m, for 25 h averages under a variety of July 2004 upwelling conditions (n = 4). Results from dilution experiments in the plume (salinity < 31.5) are plotted according to distance from the mouth. Dilution experiments in oceanic salinities (>31.5) or >80 km from the river mouth are shown in aggregate to the right of the distance axis: under the assumptions used to determine

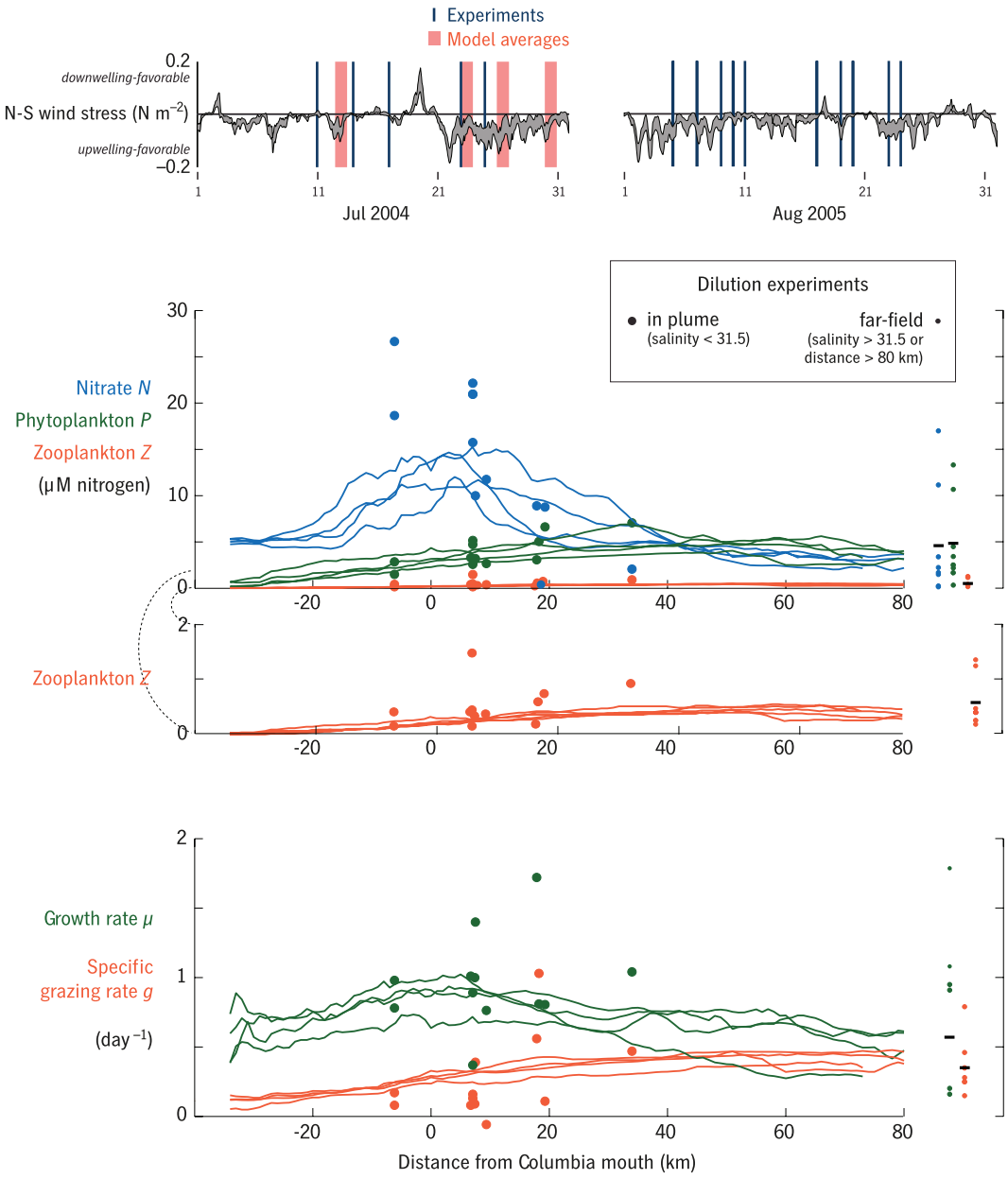

Figure 8. Stocks and rates at 0–5 m depth along the plume axis. Four 25 h model averages under a variety of upwelling conditions are shown, along with data from dilution experiments in the plume (salinity < 31.5 psu; plotted versus distance) and in the oceanic far-field (salinity > 31.5 psu, or >80 km from the river mouth; small dots). Means of far-field data are marked by black bars. Times of experiments and model averages are marked on a wind stress time series.

model rate parameters in section 2.6, we expect profiles along the plume axis to converge on the average of these far-field oceanic data for each variable.

[43] The model under-predicts the highest nitrate concentrations seen but correctly (and perhaps unsurprisingly) places the nutrient maximum at the mouth of the estuary. The model reproduces the falloff of nutrient values from the near-field plume (~10 km from the mouth) to the oceanic far-field condition (80 km), with error comparable to the variability between events seen in the data. The same is true for the profiles of phytoplankton and zooplankton biomass, which match observations well in both estuary and plume. Growth and grazing rates are much more variable in the observations than in the model: this indicates, perhaps, how much of the empirical variability is due to changing species composition and unmodeled biological processes, rather than interaction between gross biological timescales and the physics. Nevertheless, the mean phytoplankton growth rate in the near-field plume is statistically indistinguishable between model and data. Modeled grazing rates are too high by approximately one standard deviation in the estuary and near-field plume, but converge on the mean of the data (as required by our parameter-choosing method) in the midfield-to-far-field plume (>15 km).

[44] Another view of the model's rate predictions is shown in Figure 9. Growth rates plotted against grazing

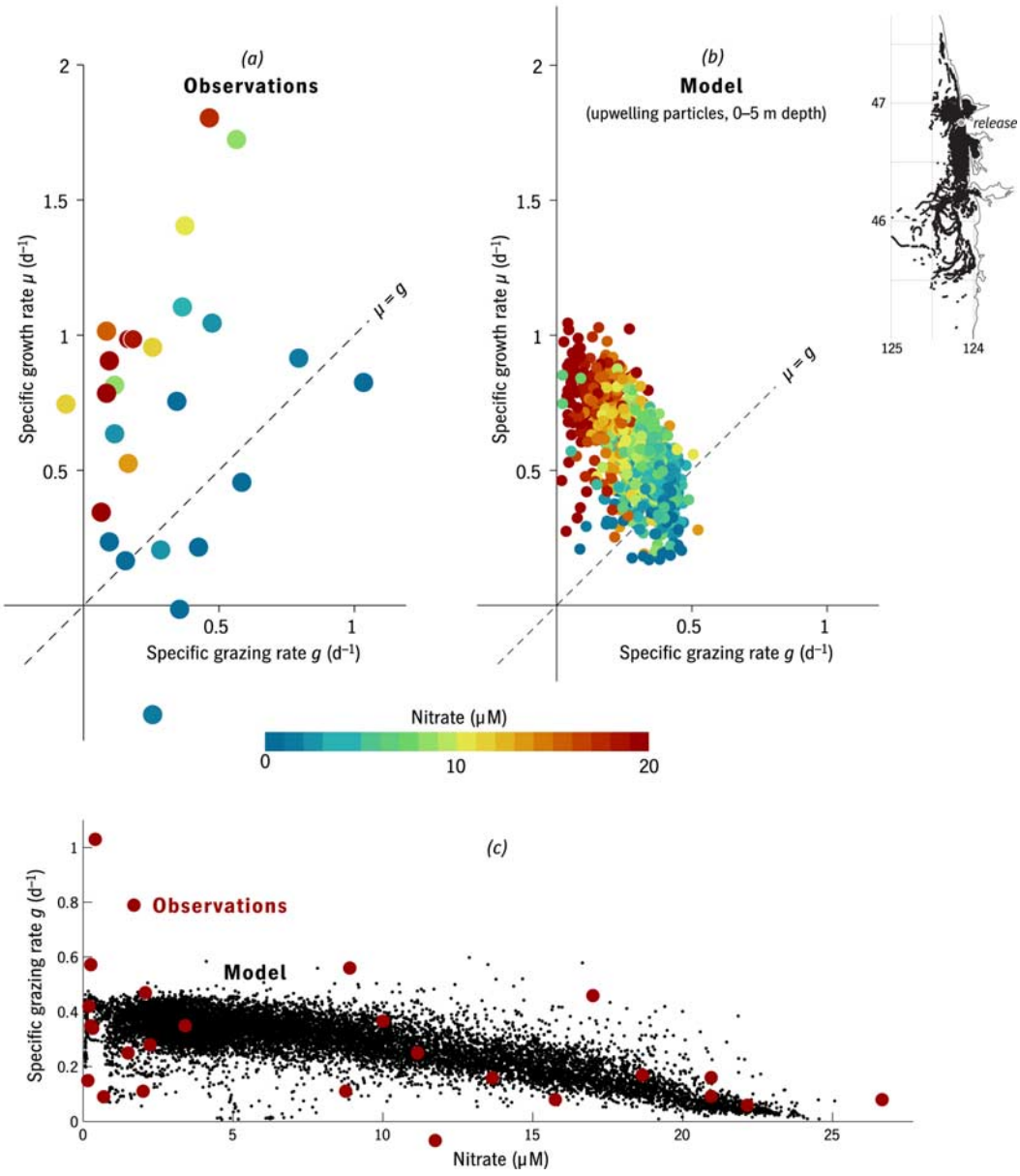

Figure 9. Growth grazing–nitrate relationship from (a) dilution experiments (reprinted from Figure 2) and (b) model particles released at the coast (gray dot) under high-nitrate (upwelling) conditions and tracked for 15 days. Particles are tracked in 3-D; model fields are sampled wherever particles are found above 5 m depth. (c) Results from Figures 9a and 9b replotted to demonstrate that the model reproduces the central tendency of the indirect relationship between grazing rate and nutrient concentration.

rates and color-coded by nutrient concentration (the matching view of the dilution data from Figure 2 is replotted in Figure 9a to ease comparison) are shown along particle paths that start at the 15 m isobath along the Washington coast (46.83°N) and traverse the study area. Particles were released continuously at the surface and tracked in three dimensions, including vertical dispersion (see *Banas et al.* [2009] for details); only particles released during upwelling conditions (initial nutrients > 10 μM) are shown, and only when found in the upper 5 m. The community time evolution seen along these paths (Figure 9b) in these conditions lies agreeably within the variability seen in the dilution data (Figure 9a). These results have been replotted in Figure 9c for a more quantitative view. The model reproduces the central tendency of the relationship seen in the dilution data between grazing rate and nitrate concentration. There is no direct relationship between these: this is, rather, a validation that the model is capturing the relationship between two community rates, the rate at which a phytoplankton population draws down upwelling-derived nutrients and the rate at which the grazer population rises to crop this new production.

3.4. Importance of Microzooplankton

[45] Our model thus has mechanistic success (Figures 8 and 9) using microzooplankton rate parameters

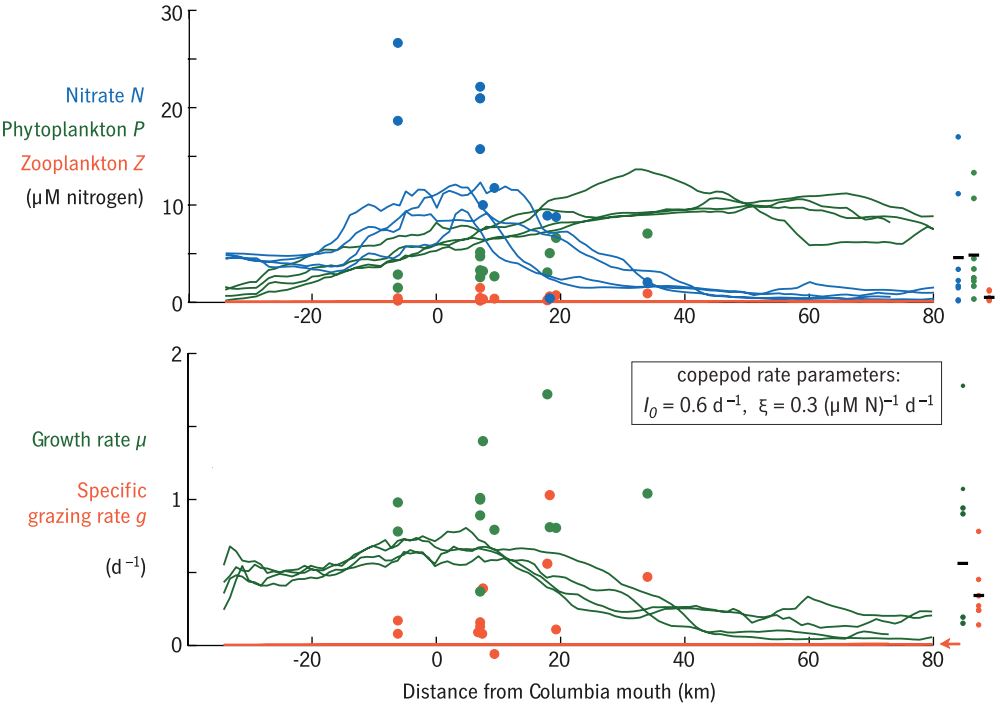

Figure 10. Stocks and rates along the plume axis for an alternate parameterization in which community-standard, copepod-inspired ingestion and mortality rates were used in place of empirical, microzooplankton rates. Model results and dilution experiment data are as in Figure 8. On this scale, grazing rates are barely distinguishable from the horizontal axis (red arrow), inconsistent with observations (small red dots).

in accordance with observations. Notably, it does not have the same success using community-standard, copepod-inspired rate parameters. As a test, we replaced the I_0 and ξ determined from dilution data in section 2.6 with values that match the "small copepod" rates used by *Spitz et al.* [2005] in their model of the Oregon upwelling system (that study uses a different functional form for grazing; I_0 was chosen to minimize the difference between overall curves). Results are shown in Figure 10. Stocks of nutrients and chlorophyll change only moderately (a factor of two in the far-field), and this change could likely be reduced by tuning other parameters or boundary conditions. Grazing rates, however, fall as one would expect by an order of magnitude. Far-field phytoplankton growth rates fall by a factor of three; they would fall farther, except that now phytoplankton growth is balanced by the "other mortality" term mP, rather than the explicitly modeled grazing term $I(P)Z$ (equation (3a)).

[46] Two conclusions can be drawn. First, if microzooplankton are omitted from a model of a system in which they are in fact important, then model predictions of rates and fluxes are extremely unreliable, but the error may not be apparent from nutrient and chlorophyll data alone. Second, when microzooplankton are improperly omitted, their ecosystem function may simply be transferred, coarsely, onto the traditional, catch all "other mortality" term. This may be one reason why NPZ models are often found to be sensitive to the phytoplankton mortality rate (m), which is never well constrained by data.

[47] Further methodological conclusions from this study are drawn in section 5 below. First, we will return to our motivating questions concerning the role of the Columbia River plume in this ecosystem.

4. Results

4.1. Controls on Phytoplankton Growth

[48] Both Figures 8 and 9 show a transition from nearly maximal phytoplankton growth, abundant nutrients, and weak grazing inshore (at the coastal wall and in the outer Columbia estuary) to depleted nutrients, an aged community with stronger grazing, and reduced phytoplankton growth in the far-field. We can quantify these patterns, and isolate the role of the Columbia plume, by mapping the fields of nutrient and grazer limitation with and without the Columbia River included in the model.

[49] Results are shown in Figure 11. Model stocks and fluxes were averaged over the top 5 m and over all of July 2004. Nutrient limitation is represented by the term $N/(k_s + N)$ which appears in equation (4). Grazing limitation is represented by g/μ, the fraction of individual phytoplankton growth μ that is cropped rather than becoming net phytoplankton population growth $\partial P/\partial t$ (see equation (2)). On average, the phytoplankton population crosses into 50% nutrient limitation near the 100 m isobath, 10–30 km offshore. The near-field plume, however, creates a localized zone of nearly maximal growth that extends onto the outer shelf.

[50] Grazing limitation is much stronger off Oregon, where is it almost uniformly >50%, than off Washington. This along-coast gradient is provocative but it could be simply a consequence of how we posed the model problem.

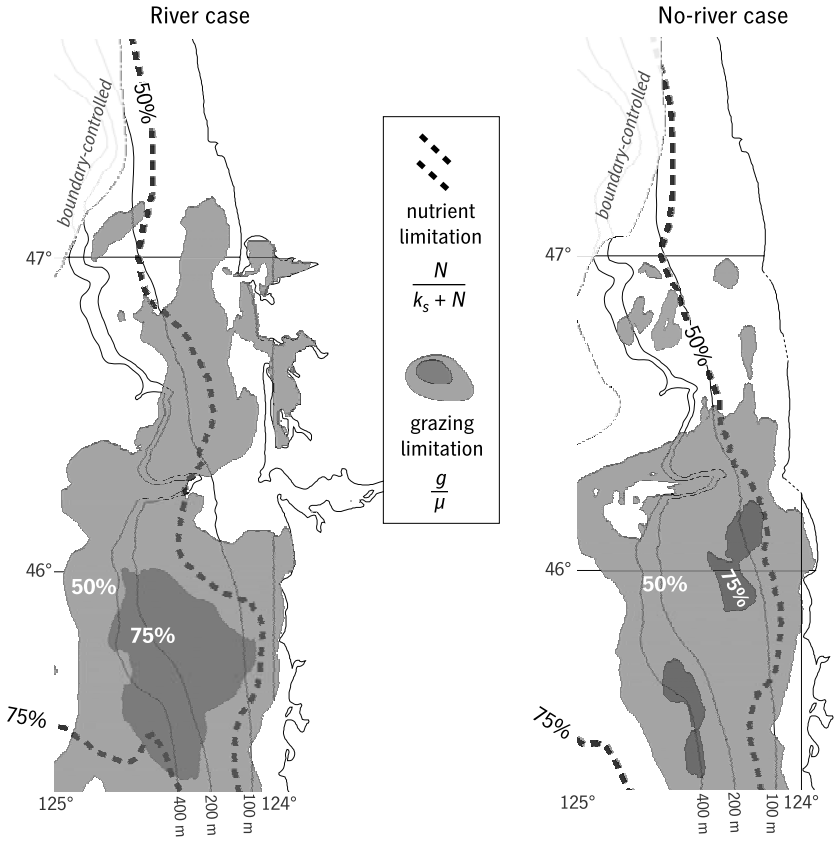

Figure 11. Regions where nutrients (dashed contours) and grazing (shaded areas) are limiting to net phytoplankton population growth in the time mean of the hindcast period. Results are shown for (left) the base case, with the Columbia River included, and (right) an alternate scenario in which the Columbia River and Washington estuaries are omitted.

Since by our choice of boundary conditions (see section 2.4) we are modeling only the biological production that occurs within the study area, we would expect the plankton community to mature into grazing limitation progressively toward the south. Still, note that the northern, boundary condition–controlled swath of the model seen as a lack of biomass in Figure 6 only passes through a corner of the area shown in Figure 11, and the model predicts chlorophyll accurately on the Washington coast south of this (Figures 6 and 7). Thus there is no evidence that the model has underestimated grazing on the Washington coast, nor, given that the model actually overestimates chlorophyll off of Oregon (Figure 7), is there evidence that the strong grazing limitation seen there (Figure 11) should be lower. Indeed, field observations based on >100 dilution experiments showed that on average, grazing limitation g/μ is higher off Oregon (E. J. Lessard et al., Phytoplankton growth and microzooplankton grazing dynamics on the Washington and Oregon coasts, manuscript in preparation, 2009; E. J. Lessard and E. R. Frame, The influence of the Columbia River plume on patterns of phytoplankton growth, grazing and chlorophyll on the Washington and Oregon coasts, paper presented at 2008 Ocean Sciences Meeting, American Society of Limnology and Oceanography, Orlando, Florida, 2008). The results from a series of grow-out experiments [*Kudela and Peterson*, 2009] are also consistent with higher grazing impact off Oregon. These model results suggest that such a pattern could arise because of circulational, rather than biological, differences between Oregon and Washington waters.

4.2. Role of the Columbia River

[51] To assess the role of the Columbia plume in shaping these patterns, we can compare the base model case with an alternate model case (Figure 11b), in which the Columbia River and the Washington estuaries (Grays Harbor and Willapa Bay) are omitted and replaced by an unbroken coastline. As one would expect, in the absence of the Columbia outflow the zone of unlimited growth near the river mouth does not appear: nutrient limitation passes the 50% level near the 100 m isobath over the entire span of the study area. The most notable difference is a reduction in grazing limitation, both north and south of the river mouth but proportionally strongest off of Washington. This is a result of the plume's bidirectionality, and the increased northward advection that the plume causes during downwelling events [*Banas et al.*, 2009]. Washington coastal production that would otherwise (in the absence of the plume) rapidly advect away to the south is instead retained off of Washington by plume reversals long enough for a strong grazer community to develop. A similar process may boost retention times and grazing impact off Oregon (Figure 11a).

[52] The timeline of chlorophyll and nutrients in Figure 12 shows this retention process in more detail. Snapshot comparisons of 0–5 m chlorophyll and 0–5 m nutrients

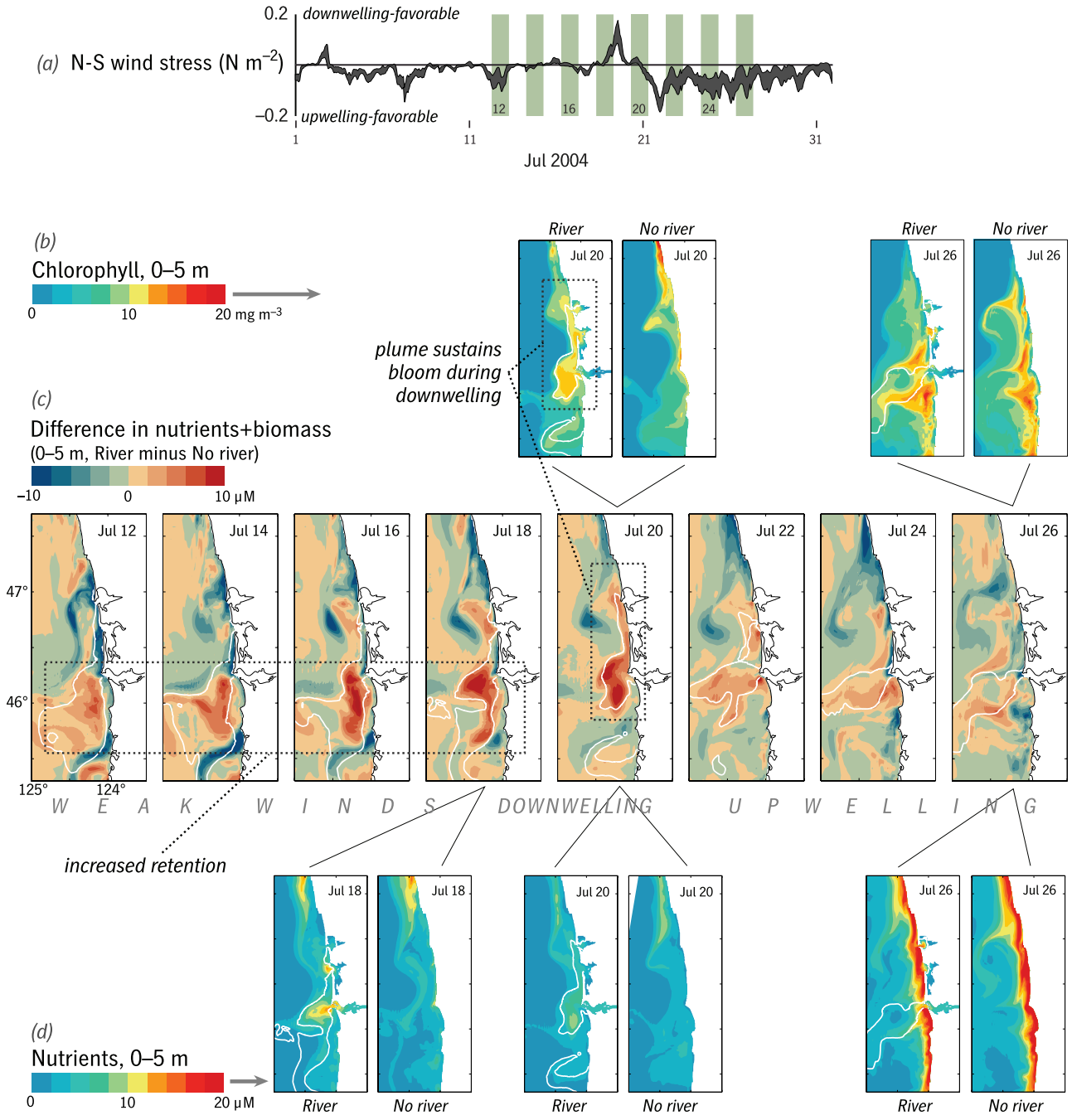

Figure 12. Timeline of nutrients and biomass in the surface layer (0–5 m average) from July 2004, from the model base case ("River"), and a case with the Columbia River and Washington estuaries omitted ("No river"). Each frame is a 25 h tidal average. The 30 psu isohaline is shown in white to indicate the location of the plume. (a) North-south wind stress is given. (c) The main timeline shows the difference between model cases in total nitrogen $N + P$; snapshots of (b) chlorophyll and (d) nutrients are also shown. Adapted from *Hickey and Banas* [2008, Figure 9], with permission from The Oceanography Society.

from the river and no-river cases are shown in Figures 12b and 12d; the main timeline in Figure 12c shows the anomaly in total nitrogen $N + P$. Under variable winds and weak upwelling (12–18 July), a positive anomaly (i.e., higher nitrogen in the presence of the plume) develops in the near-field-to-midfield plume, strongest in the bulge region but extending over 150 km into Washington and Oregon shelf waters by 18 July. During the downwelling event on 20 July, the higher-nitrogen zone is coextensive with the northward plume, and supports a strong phytoplankton bloom in the river case, in contrast to the no-river case in which both nutrients (Figure 12d) and biomass (Figure 12b) are low. Note that a third model case (not shown), in which the river is included but the 5 μM N carried by the river in the base

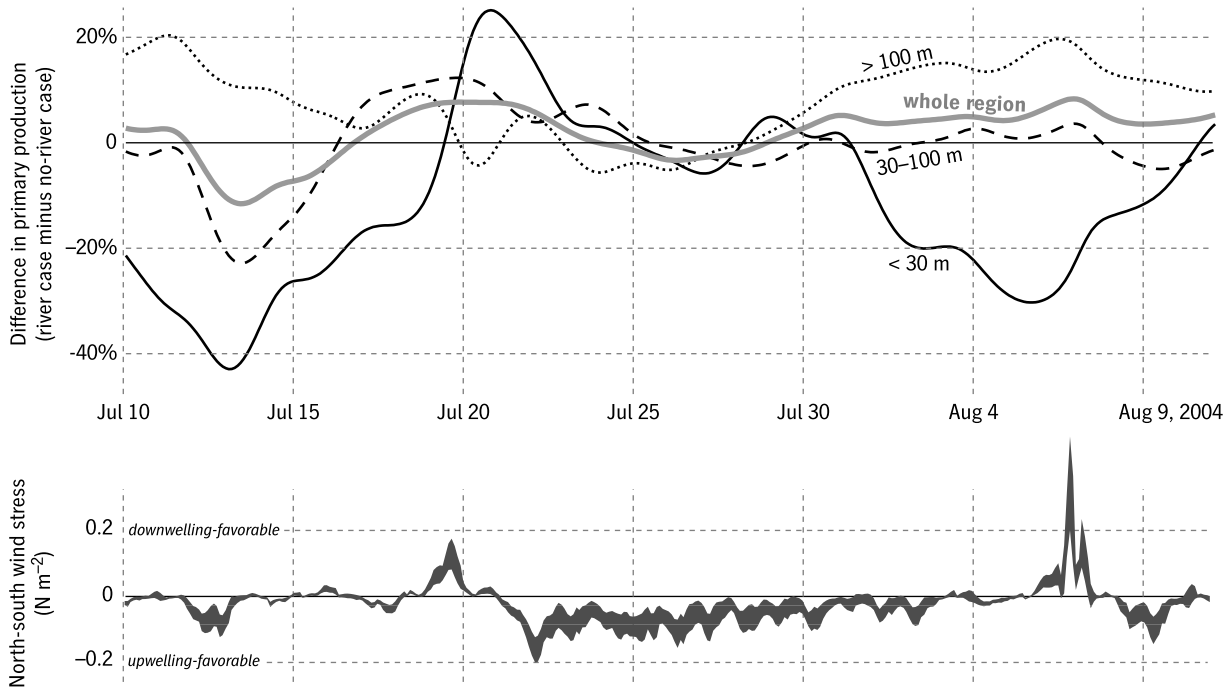

Figure 13. Difference in integrated primary production between model cases with and without the Columbia River and Washington estuaries included, correlated with wind stress. Relative change in primary production (river case minus no-river case) is shown for the entire region between 45.5°N and 47°N and for three subregions: the inner shelf (depths < 30 m), the midshelf (30–100 m), and the outer shelf and slope (>100 m). Tidal and diurnal signals have been removed with a 48 h low-pass filter.

case is omitted, is much closer to the base river case than to the no-river case during this period, with undepleted nutrient stocks and chlorophyll >10 mg m^{-3} during the downwelling event. This confirms that the pattern labeled "increased retention" in Figure 12c is indeed an effect of retention, not dependent on direct supply of watershed nutrients.

[53] This retention pattern weakens and breaks apart as upwelling returns (Figure 12) (22–26 July), until on 26 July patterns of biomass and nutrients are qualitatively similar between the river and no-river cases, plume circulation effects overwhelmed by strong southward and offshore advection. Thus the retention process described above is, like the other circulational plume effects described by *Banas et al.* [2009], episodic and dependent on the variability of the wind, not freshwater dynamics alone.

[54] A second, more subtle effect of the plume, not apparent from these snapshots or the long time average in Figure 11, can be seen when we average model fluxes in space with more precision. A tidally averaged time series of the difference in integrated primary production between the base model case and the no-river case is shown in Figure 13. Results are shown for the entire region between 45.5°N and 47°N out to 125°W, and three subranges: the inner shelf (depths <30 m, not including the estuaries), the mid shelf (30–100 m), and the outer shelf and slope (>100 m). During the sustained, strong upwelling event depicted in Figures 5, 6, and 7 (22–29 July), differences between the two cases are negligible, but under weak and variable winds greater differences develop. From 10 July until the downwelling event on 19 July, and again from 1 August until the downwelling event on 7 August, primary production is shifted offshore by plume dynamics. During these time periods, primary production is ~20% lower in the river case on the inner shelf and 10–20% higher on the outer shelf and slope. This pattern may be caused by seaward advection of nutrients or seaward advection of biomass; in general, both probably occur, at different times depending on the recent time history of the system.

[55] What we have labeled "increased retention" during the weak wind period 12–18 July (Figure 12c) may in fact consist of export from a narrow band on the inner shelf into deeper water and retention there, i.e., the creation of offshore storage features which then advect back onto the inner shelf during downwelling (20 July) (Figures 12 and 13). *Banas et al.* [2009] likewise documented the plume's creation of transient recirculation features whose short-term, local effect is retention but whose net statistical effect is to dispersively export water from the upwelling zone into deeper water. The pattern depicted in Figure 13 is confirmation of our original hypothesis, that this plume-driven, episodic cross-shelf export would be reflected in patterns of biological production.

5. Conclusions

5.1. Large-Scale Biological Effects of the Columbia River Plume

[56] *Banas et al.* [2009] reported that the bidirectional, laterally dispersive Columbia River plume acted as (1) a cross-shelf exporter and (2) a semipermeable along-coast barrier. In this study we see biological consequences of both parts of this pattern.

[57] First, in the cross-shelf direction, plume dynamics shift ~20% of inner shelf primary production to deeper water under weak or variable upwelling (Figure 13). The magnitude of this cross-shelf biomass export is quantitatively similar to the hydrodynamic export determined by *Banas et al.* [2009] from intensive particle tracking, further suggesting that the mechanism is the same. Under strong, sustained upwelling, plume dynamics have a much smaller effect on patterns of primary production (<5%): the offshore shift described here appears to rely on an interaction between plume dynamics and wind intermittency.

[58] Second, in the along-coast direction, we found that the presence of the plume shifted both Oregon and (more dramatically) Washington offshore waters toward higher grazing limitation, a consequence of longer retention times (Figure 11). A background north-to-south gradient in grazing intensity g/μ was also seen in both river and no-river cases, but this result is equivocal and may be an artifact of the model design, as discussed in section 3.2.

5.2. A Strategy for Ecosystem Model Design

[59] As a simulation of chlorophyll and nutrient patterns, our ecosystem model has moderate predictive power (correlation coefficients 0.41–0.87) (Table 3). Our goal was not point-by-point simulation, however, but rather mechanistic validity, the confidence in model pathways necessary to support faith in descriptions of ecosystem function and hypothetical scenarios like the no-river case (Figures 11, 12, and 13). We found that a very simple NPZD model can in fact pass comprehensive, mechanistic validation tests involving not just stocks but intrinsic rates (tests that are rarely attempted), provided two things.

[60] First, one needs diverse biological observations: not just nutrients and chlorophyll, but rate and flux data, gross taxonomic identification, and parameter-constraining process studies that minimize the reliance on literature values. A handful of empirical grazing rates may be worth as much to a modeling effort as hundreds of chlorophyll measurements.

[61] Second, one must treat the free parameters as part of the conceptual model. There is a relatively extensive literature analyzing the functional forms used for flux terms in simple ecosystem models [e.g., *Edwards and Yool*, 2000; *Fulton et al.*, 2003; *Gentleman et al.*, 2003]. In contrast, choosing parameters values is often left to mathematical, not biological, reasoning. In some cases this may be inescapable, and indeed we have left a number of regeneration-pathway parameters to modeling tradition, for lack of local data (Table 1). But we have shown that to read the model equations as specific hypotheses about population ecology (section 2.6) requires particular parameter values. If we used a different zooplankton mortality rate, for example, we would be making a qualitatively different hypothesis about far-field population dynamics. This is an opportunity as well as a burden, since it allows us to diagnose hard-to-measure parameters like zooplankton mortality from field data.

5.3. Importance of Microzooplankton

[62] *Edwards et al.* [2000] showed that the choice of macrozooplankton or microzooplankton rates makes qualitative differences to the results of NPZ models in upwelling systems, but many single-Z-compartment models have continued to use copepod-inspired values. (*Hood et al.* [2001] is an exception.) *Edwards* [2001] reports 0.6–1.4 d^{-1} as the range of maximum zooplankton ingestion rates used "in a variety of other models." Our ingestion rate of 4.8 d^{-1} is far outside that range but unremarkable within the range of laboratory values for dinoflagellates and ciliates reported by *Hansen et al.* [1997]. There is no universally correct value for these parameters: in every model study, values should be chosen to implement specific, local hypotheses. But *Calbet and Landry* [2004] report that microzooplankton consume 60% of primary production in coastal zones and even more in the open ocean and tropical/subtropical systems. It may be possible for some applications to find alternate, implicit means to parameterize the microbial loop [e.g., *Steele*, 1998] but in our informal survey of the single-Z-compartment NPZ modeling literature, such reasoning remains uncommon. In short, it appears that the microbial revolution in biological oceanography still has not penetrated far enough into the ecosystem modeling community.

[63] There is a trend in the community toward multiple-Z-compartment models (often, a microzooplankton compartment and a mesozooplankton compartment) for just these reasons. Nevertheless, *Friedrichs et al.* [2007] showed that multiple-Z models did not in general perform better than single-Z ones in systematic skill assessments, probably because of mismatch between the variety of model architectures and the single set of zooplankton biomass data used for assimilation. Thus it appears that the crucial issue is not model complexity per se, but close coordination between observations and model development. *Flynn* [2005] has commented on the human dimensions of this problem. Our results suggest, encouragingly, that representing the role of microzooplankton more accurately does not require great model complexity, and in fact can breathe new life into old tools like the four-box NPZD model.

[64] **Acknowledgments.** This work was supported by NSF grants OCE 0239089 and OCE 0238347. This is contribution 33 of the NSF CoOP River Influences on Shelf Ecosystems (RISE) program. Many thanks to the captain and crew of the R/V *Wecoma* and the other participants in the RISE1 and RISE3 cruises and a special thanks to Ken Bruland, Maeve Lohan, and Tina Sohst for the nutrient data. Thanks as well to programmer and computer cluster administrator David Darr. The thoughtful input of Peter Franks, Chris Edwards, Yvette Spitz, and Andy Leising during the model design phase; Yonggang Liu during the validation phase; and Marjy Friedrichs and an anonymous reviewer during the revision process has been much appreciated.

References

Arhonditsis, G. B., and M. T. Brett (2004), Evaluation of the current state of mechanistic aquatic biogeochemical cycling, *Mar. Ecol. Prog. Ser.*, *271*, 13–26, doi:10.3354/meps271013.

Banas, N. S., P. MacCready, and B. M. Hickey (2009), The Columbia River plume as along-shelf barrier and cross-shelf exporter: A Lagrangian model study, *Cont. Shelf Res.*, *29*, 292–301, doi:10.1016/j.csr.2008.03.011.

Barron, C. N., A. B. Kara, P. J. Martin, R. C. Rhodes, and L. F. Smedstad (2006), Formulation, implementation and examination of vertical coordinate choices in the Global Navy Coastal Ocean Model (NCOM), *Ocean Modell.*, *11*, 347–375, doi:10.1016/j.ocemod.2005.01.004.

Batchelder, H. P., C. A. Edwards, and T. M. Powell (2002), Individual-based models of copepod populations in coastal upwelling regions: Implications of physiologically and environmentally influenced diel vertical migration on demographic success and nearshore retention, *Prog. Oceanogr.*, *53*, 307–333, doi:10.1016/S0079-6611(02)00035-6.

Botsford, L. W., C. A. Lawrence, E. P. Dever, A. Hastings, and J. Largier (2006), Effects of variable winds on biological productivity on continental shelves in coastal upwelling systems, *Deep Sea Res., Part II*, *53*, 25–26.

Bruland, K. W., M. C. Lohan, A. M. Aguilar-Islas, G. J. Smith, B. Sohst, and A. Baptista (2008), Factors influencing the chemistry of the near-field Columbia River plume: Nitrate, silicic acid, dissolved Fe, and dissolved Mn, *J. Geophys. Res.*, *113*, C00B02, doi:10.1029/2007JC004702.

Calbet, A., and M. R. Landry (2004), Phytoplankton growth, microzooplankton grazing, and carbon cycling in marine systems, *Limnol. Oceanogr.*, *49*, 51–57.

Canuto, V. M., A. Howard, Y. Cheng, and M. S. Dubovikov (2001), Ocean turbulence. Part I: One-point closure model — Momentum and heat vertical diffusivities, *J. Phys. Oceanogr.*, *31*, 1413–1426, doi:10.1175/1520-0485(2001)031<1413:OTPIOP>2.0.CO;2.

Denman, K. L., and M. A. Peña (1999), A coupled 1-D biological/physical model of the northeast subarctic Pacific Ocean with iron limitation, *Deep Sea Res., Part II*, *46*, 2877–2908, doi:10.1016/S0967-0645(99)00087-9.

Edwards, A. M. (2001), Adding detritus to a nutrient-phytoplankton-zooplankton model: A dynamical-systems approach, *J. Plankton Res.*, *23*, 389–413, doi:10.1093/plankt/23.4.389.

Edwards, A. M., and A. Yool (2000), The role of higher predation in plankton population models, *J. Plankton Res.*, *22*, 1085–1112, doi:10.1093/plankt/22.6.1085.

Edwards, C. A., H. P. Batchelder, and T. M. Powell (2000), Modeling microzooplankton and macrozooplankton dynamics within a coastal upwelling system, *J. Plankton Res.*, *22*, 1619–1648, doi:10.1093/plankt/22.9.1619.

Egbert, G. D., and S. Y. Erofeeva (2002), Efficient inverse modeling of barotropic ocean tides, *J. Atmos. Oceanic Technol.*, *19*, 183–204.

Egbert, G., A. Bennett, and M. Foreman (1994), TOPEX/Poseidon tides estimated using a global inverse model, *J. Geophys. Res.*, *99*, 24,821–24,852, doi:10.1029/94JC01894.

Fennel, K., M. Losch, J. Schroter, and M. Wenzel (2001), Testing a marine ecosystem model: Sensitivity analysis and parameter optimization, *J. Mar. Syst.*, *28*, 45–63, doi:10.1016/S0924-7963(00)00083-X.

Flynn, K. F. (2005), Castles built on sand: Dysfunctionality in plankton models and the inadequacy of dialogue between biologists and modellers, *J. Plankton Res.*, *27*, 1205–1210, doi:10.1093/plankt/fbi099.

Frame, E. R., and E. J. Lessard (2009), Does the Columbia River plume influence phytoplankton community structure along the Washington and Oregon coasts?, *J. Geophys. Res.*, doi:10.1029/2008JC004999, in press.

Franks, P. J. S. (2002), NPZ models of plankton dynamics: Their construction, coupling to physics, and application, *J. Oceanogr.*, *58*, 379–387, doi:10.1023/A:1015874028196.

Friedrichs, M. A. M., et al. (2007), Assessment of skill and portability in regional marine biogeochemical models: Role of multiple planktonic groups, *J. Geophys. Res.*, *112*, C08001, doi:10.1029/2006JC003852.

Fulton, E. A., A. D. M. Smith, and C. R. Johnson (2003), Mortality and predation in ecosystem models: Is it important how these are expressed?, *Ecol. Modell.*, *169*, 157–178, doi:10.1016/S0304-3800(03)00268-0.

Gentleman, W. (2002), A chronology of plankton dynamics in silico: How computer models have been used to study marine ecosystems, *Hydrobiologia*, *480*, 69–85, doi:10.1023/A:1021289119442.

Gentleman, W., A. Leising, B. Frost, S. Strom, and J. Murray (2003), Functional responses for zooplankton feeding on multiple resources: A review of assumptions and biological dynamics, *Deep Sea Res., Part II*, *50*, 2847–2875, doi:10.1016/j.dsr2.2003.07.001.

Haidvogel, D. B., H. G. Arango, K. Hedstrom, A. Beckmann, P. Malanotte-Rizzoli, and A. F. Shchepetkin (2000), Model evaluation experiments in the North Atlantic Basin: Simulations in nonlinear terrain-following coordinates, *Dyn. Atmos. Oceans*, *32*, 239–281, doi:10.1016/S0377-0265(00)00049-X.

Halliwell, G. R., and J. S. Allen (1984), Large scale sea level response to atmospheric forcing along the west coast of North America, summer, 1973, *J. Phys. Oceanogr.*, *14*, 864–886, doi:10.1175/1520-0485(1984)014<0864:LSSLRT>2.0.CO;2.

Hansen, J., P. K. Bjornsen, and B. W. Hansen (1997), Zooplankton grazing and growth: Scaling within the 2–2000 μm body size range, *Limnol. Oceanogr.*, *42*, 687–704.

Hickey, B. M. (1989), Patterns and processes of circulation over the shelf and slope, in *Coastal Oceanography of Washington and Oregon*, edited by B. M. Hickey and M. R. Landry, pp. 41–115, Elsevier Sci., Amsterdam.

Hickey, B. M., and N. S. Banas (2003), Oceanography of the U. S. Pacific Northwest coastal ocean and estuaries with application to coastal ecology, *Estuaries*, *26*, 1010–1031, doi:10.1007/BF02803360.

Hickey, B. M., and N. S. Banas (2008), Why is the northern end of the California Current System so productive?, *Oceanography (Wash. D. C.)*, *21*(4), 90–107.

Hickey, B. M., S. Geier, N. Kachel, and A. MacFadyen (2005), A bi-directional river plume: The Columbia in summer, *Cont. Shelf Res.*, *25*, 1631–1656, doi:10.1016/j.csr.2005.04.010.

Hickey, B. M., R. McCabe, R. M. Kudela, E. P. Dever, and S. Geier (2009), Three interacting freshwater plumes in the northern California Current System, *J. Geophys. Res.*, *114*, C00B03, doi:10.1029/2008JC004907.

Hood, R. R., N. R. Bates, D. G. Capone, and D. B. Olson (2001), Modeling the effect of nitrogen fixation on carbon and nitrogen fluxes at BATS, *Deep Sea Res., Part II*, *48*, 1609–1648, doi:10.1016/S0967-0645(00)00160-0.

Horner-Devine, A. R. (2008), The bulge circulation in the Columbia River plume, *Cont. Shelf Res.*, *29*, 234–251, doi:10.1016/j.csr.2007.12.012.

Kara, A. B., C. N. Barron, P. J. Martin, L. F. Smedstad, and R. C. Rhodes (2006), Validation of interannual simulations from the 1/8 degree global Navy Coastal Ocean Model (NCOM), *Ocean Modell.*, *11*, 376–398, doi:10.1016/j.ocemod.2005.01.003.

Kudela, R. M., and T. D. Peterson (2009), Influence of a buoyant river plume on phytoplankton nutrient dynamics: What controls standing stocks and productivity?, *J. Geophys. Res.*, doi:10.1029/2008JC004913, in press.

Landry, M. R., and R. P. Hassett (1982), Estimating the grazing impact of marine micro-zooplankton, *Mar. Biol. Berlin*, *67*, 283–288, doi:10.1007/BF00397668.

Leising, A. W., J. J. Pierson, C. Halsband-Lenk, R. Horner, and J. Postel (2005), Copepod grazing during spring blooms: Can *Pseudocalanus newmani* induce trophic cascades?, *Prog. Oceanogr.*, *67*, 406–421, doi:10.1016/j.pocean.2005.09.009.

Lessard, E. J., and M. C. Murrell (1996), Distribution, abundance and size composition of heterotrophic dinoflagellates and ciliates in the subtropical Sargasso Sea, *Deep Sea Res., Part I*, *43*, 1045–1065, doi:10.1016/0967-0637(96)00052-0.

Liu, Y., P. MacCready, B. M. Hickey, E. P. Dever, P. M. Kosro, and N. S. Banas (2009), Evaluation of a coastal ocean circulation model for the Columbia River plume in summer 2004, *J. Geophys. Res.*, *114*, C00B04, doi:10.1029/2008JC004929.

Lohan, M. C., and K. W. Bruland (2006), Importance of vertical mixing for additional sources of nitrate and iron to surface waters of the Columbia River plume: Implications for biology, *Mar. Chem.*, *98*, 260–273, doi:10.1016/j.marchem.2005.10.003.

MacCready, P., N. S. Banas, B. M. Hickey, and E. P. Dever (2009), A model study of tide- and wind-induced mixing in the Columbia River estuary and plume, *Cont. Shelf Res.*, *29*, 278–291, doi:10.1016/j.csr.2008.03.015.

MacFadyen, A., B. M. Hickey, and M. G. G. Foreman (2005), Transport of surface waters from the Juan de Fuca eddy region to the Washington coast, *Cont. Shelf Res.*, *25*, 2008–2021, doi:10.1016/j.csr.2005.07.005.

Mass, C. F., et al. (2003), Regional environmental prediction over the Pacific Northwest, *Bull. Am. Meteorol. Soc.*, *84*, 1353–1366, doi:10.1175/BAMS-84-10-1353.

Menden-Deuer, S., and E. J. Lessard (2000), Carbon to volume relationships for dinoflagellates, diatoms, and other protist plankton, *Limnol. Oceanogr.*, *45*, 569–579.

Olson, M. B., E. J. Lessard, C. H. J. Wong, and M. J. Bernhardt (2006), Copepod feeding selectivity on microplankton, including the toxigenic diatoms *Pseudo-nitzschia* spp., in the coastal Pacific Northwest, *Mar. Ecol. Prog. Ser.*, *326*, 207–220, doi:10.3354/meps326207.

Olson, M. B., E. J. Lessard, W. P. Cochlan, and V. L. Trainer (2008), Intrinsic growth and microzooplankton grazing on toxigenic *Pseudo-nitzschia* spp. diatoms from the coastal northeast Pacific, *Limnol. Oceanogr.*, *53*, 1352–1368.

Putt, M., and D. K. Stoecker (1989), An experimentally determined carbon:volume ratio for marine "oligotrichous" ciliates from estuarine and coastal waters, *Limnol. Oceanogr.*, *34*, 1097–1103.

Roff, J. C., and R. R. Hopcroft (1986), High precision microcomputer based measuring system for ecological research, *Can. J. Fish. Aquat. Sci.*, *43*, 2044–2048.

Spitz, Y. H., P. A. Newberger, and J. S. Allen (2003), Ecosystem response to upwelling off the Oregon coast: Behavior of three nitrogen-based models, *J. Geophys. Res.*, *108*(C3), 3062, doi:10.1029/2001JC001181.

Spitz, Y. H., J. S. Allen, and J. Gan (2005), Modeling of ecosystem processes on the Oregon shelf during the 2001 summer upwelling, *J. Geophys. Res.*, *110*, C10S17, doi:10.1029/2005JC002870.

Steele, J. H. (1998), Incorporating the microbial loop in a simple plankton model, *Proc. R. Soc. London, Ser. B*, *265*, 1771–1777, doi:10.1098/rspb.1998.0501.

Steele, J. H., and E. W. Henderson (1992), The role of predation in plankton models, *J. Plankton Res.*, *14*, 157–172.

Stoecker, D. K., and J. M. Capuzzo (1990), Predation on protozoa: Its importance to zooplankton, *J. Plankton Res.*, *12*, 891–908, doi:10.1093/plankt/12.5.891.

Tang, E. P. Y. (1995), The allometry of algal growth rates, *J. Plankton Res.*, *17*, 1325–1335.

Umlauf, L., and H. Burchard (2003), A generic length-scale equation for geophysical turbulence models, *J. Mar. Res.*, *61*, 235–265, doi:10.1357/002224003322005087.

Ware, D. M., and R. E. Thomson (2005), Bottom-up ecosystem trophic dynamics determine fish production in the northeastern Pacific, *Science*, *308*, 1280–1284, doi:10.1126/science.1109049.

Willmott, C. J. (1981), On the validation of models, *Phys. Geogr.*, *2*, 184–194.

Worden, A. Z., J. K. Nolan, and B. Palenik (2004), Assessing the dynamics and ecology of marine picophytoplankton: The importance of eukaryotic component, *Limnol. Oceanogr.*, *49*, 168–179.

N. S. Banas, Applied Physics Laboratory, University of Washington, Campus Box 355640, Seattle, WA 98195, USA. (banasn@u.washington.edu)

E. Frame, Northwest Fisheries Science Center, NOAA, 2725 Montlake Boulevard East, Seattle, WA 98112, USA.

B. M. Hickey, E. J. Lessard, and P. MacCready, School of Oceanography, University of Washington, Campus Box 355351, Seattle, WA 98195, USA.

R. M. Kudela, Ocean Sciences Department, University of California, Santa Cruz, CA 95064, USA.

T. D. Peterson, Science and Technology Center for Coastal Margin Observation and Prediction, Oregon Health and Science University, Beaverton, OR 97006, USA.